A Field Experiment to Validate Atmospheric Dispersion and Dose Model

Nielsen, Sven Poul; Gryning, Sven-Erik; Karlberg, O.; Lyck, E.; Thykier-Nielsen, Søren

Publication date:
1986

Document Version
Publisher's PDF, also known as Version of record

Risø-R-495

Risø-R-495

RISØ

A Field Experiment to Validate Atmospheric Dispersion and Dose Models

S. P. Nielsen*, S. E. Gryning*, O. Karlberg**,
E. Lyck*** and S. Thykier-Nielsen*

Risø National Laboratory, DK-4000 Roskilde, Denmark
May 1986

RISØ-R-495

DOUBLE TRACER EXPERIMENTS TO EVALUATE ATMOSPHERIC TRANSPORT AND DOSE MODELS

Sven Poul Nielsen, Sven-Erik Gryning, Olof Karlberg*),
Erik Lyck**), and Søren Thykier-Nielsen.

*) Studsvik Energiteknik AB, S-611 82 Nyköping, Sweden

**) Danish Environmental Protection Agency, Air Pollution Laboratory, Risø National Laboratory, DK-4000 Roskilde, Denmark

Abstract. Two tracers, sulphurhexafluoride (SF_6) and radioactive noble gases, were released simultaneously from a 110-m stack and detected downwind at distances of 3-4 km. The experiments were made at the Swedish nuclear power plant Ringhals in 1981. The radioactive tracer was routine emissions from unit 1 (BWR). The one-hour measurements yielded crosswind profiles at ground level of SF_6-concentrations and of gamma radiation from the plume. The measured profiles were compared to profiles calculated with computer models. The comparison showed that the models sometimes underestimate and sometimes overestimate the results, which seems to indicate that the models within their limited accuracy yield unbiased results. The ratios between measured and calculated values range from 0.2 to 3. The measurements revealed a surplus of gamma radiations from the noble gas daughters compared to those from the gases. This was interpreted as due to ground deposition and the estimated deposition velocities ranged from 2 to 10 cm/s.

(Continued on next page)

May 1986
Risø National Laboratory, DK-4000 Roskilde, Denmark

The meteorological conditions were monitored from a 100-m meteorological tower and from an 11-m mast. Measurements were made of wind speed, wind direction, and temperatures at different heights, and during each experiment a mini-radiosonde was released giving information on a possible inversion layer.

The SF_6-tracer was injected to the stack prior to the experiments. Air-samples were collected downwind in plastic bags by radio-controlled sampling units. The SF_6-concentrations in the bags were determined with gas chromatography.

Measurements of the gamma radiation from the plume were made with ionisation chambers and GM-counters. Furthermore, a few mobile gamma spectrometers were available giving information on the unscattered gamma radiation, thereby permitting identification of the radioactive isotopes.

The work was partly financed by the Nuclear Safety Board of the Swedish Utilities and by the Danish association of utilities in Jutland and on Funen, Elsam.

ISBN 87-550-1273-6
ISSN 0106-2840

Grafisk Service, Risø 1986

CONTENTS

1. INTRODUCTION

Computer models for the calculation of human exposure to ionising radiation from atmospheric releases of radioactive material have become important tools for assessment of the risk from nuclear installations. In the past, model predictions were generally believed to be conservative because a number of assumptions and parameter values were purposely intended to reduce the risk of underestimation. The probability of individuals receiving doses in excess of model predictions was considered to be very small. In the last 5-10 years there has been a tendency to reduce model conservatism and to improve predictive accuracy by incorporating more realistic assumptions and parameters. However, a model aimed at predicting average concentrations and doses may have a high probability of underestimation. Therefore, the need to evaluate the predictive capabilities of models used in radiological risk assessments is of particular importance.

Contemporary atmospheric-transport models have been developed from two main approaches: trajectory tracing, in which discrete releases are followed in the direction of the wind, and statistical models, in which the activity concentration in the plume is described as a function of distance in the direction of the wind. The statistical models are considered to be adequate for the calculation of long-term average exposures from routine releases to the atmosphere (UNSCEAR, 1982). The trajectory models are capable of tracing short-duration releases through a time-varying wind-velocity field and are thus well suited for the calculation of short-term exposures from unusual/accidental releases. However, these models require large amounts of data and involve relatively large computational expenditure.

Model intercomparisons have been made on a purely computational basis (Thykier-Nielsen et al., 1978, Thykier-Nielsen, 1979, and CSNI/NEA, 1984), which in some cases have revealed rather large

differences between model predictions. Only few experimental studies have been made to investigate the predictive capabilities of the models and these studies have mainly been concerned with long-term exposures from routine emissions of radioactive effluents.

This report presents work from an experimental campaign in 1981 at the Ringhals nuclear power plant in Sweden. The aim of the project was to obtain experimental short-term observations of concentrations and gamma-ray exposures from stack effluents and to compare these results with corresponding values calculated from computer models. Two tracers, sulphurhexafluoride (SF_6) and radioactive noble gases were used. They were released from a 110-m stack and detected at ground level downwind at distances of 3-4 km. Two Gaussian plume models were used: PLUCON and UNIDOSE. The first was developed at Risø National Laboratory, and the other at Studsvik Energiteknik AB.

2. THE EXPERIMENTAL SITE

The Ringhals nuclear power plant is situated on the Swedish west coast about 50 km south of Gothenburg. The power plant consists of a BWR unit and three PWR units. The BWR unit has a rated electric power of 760 MW. The routine release of radioactive noble gases from the stack of this unit was used as a tracer in the measurements.

The experimental site is a rather level rural area reaching about 60 m above mean sea level at its highest point. The vegetation comprises partly coniferous trees and partly agricultural fields covered with grass.

The topography and woodland distribution of the experimental site is shown in Fig. 1. Figure 2 shows the measurement line

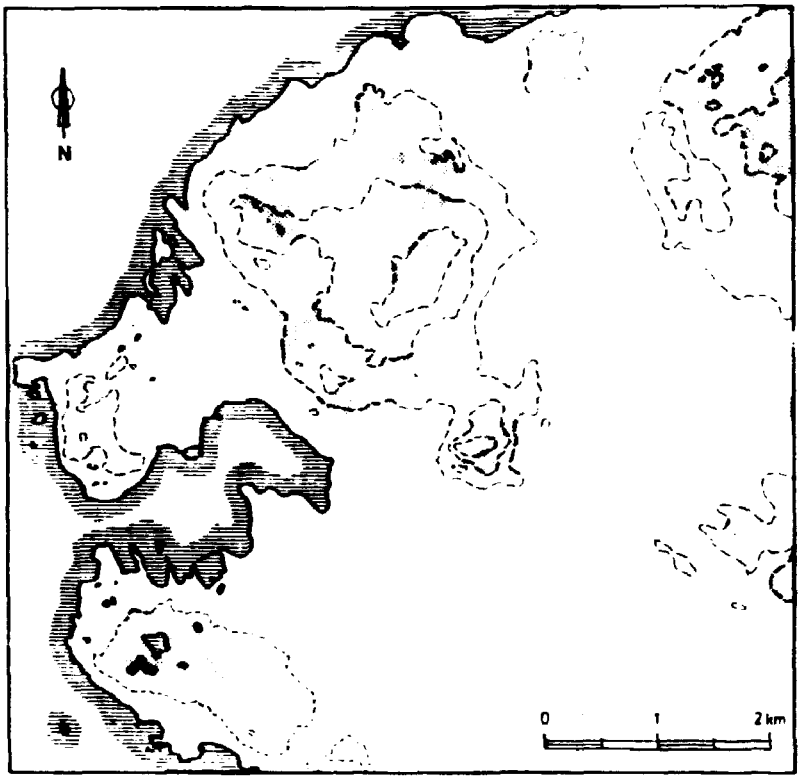

Fig.1. Map of the experimental site showing the woodland distribution (shaded areas) and the topography with contour heights for every 15 m.

circumscribing the reactor stack at a distance of 3 - 4 km. Along the measurement line 82 positions were marked out in preparation for the experiments.

3. THE EXPERIMENTAL CAMPAIGN

The experiments were planned from experience with previous measurements of noble gas releases from the Ringhals power plant (Karlberg et al., 1980) and from experience with SF_6-tracer experiments (Gryning and Lyck, 1980).

In the following a general outline of the experimental set-up is given:

The initial step was to select the crosswind measurement line to be used for the positioning of the SF_6-samplers and the gamma-ray detectors. A route accessible by car was chosen circumscribing the reactor stack at a distance of 3-4 km, Fig. 2. Along this route positions were marked out about every 150 m, yielding a total of 82 positions.

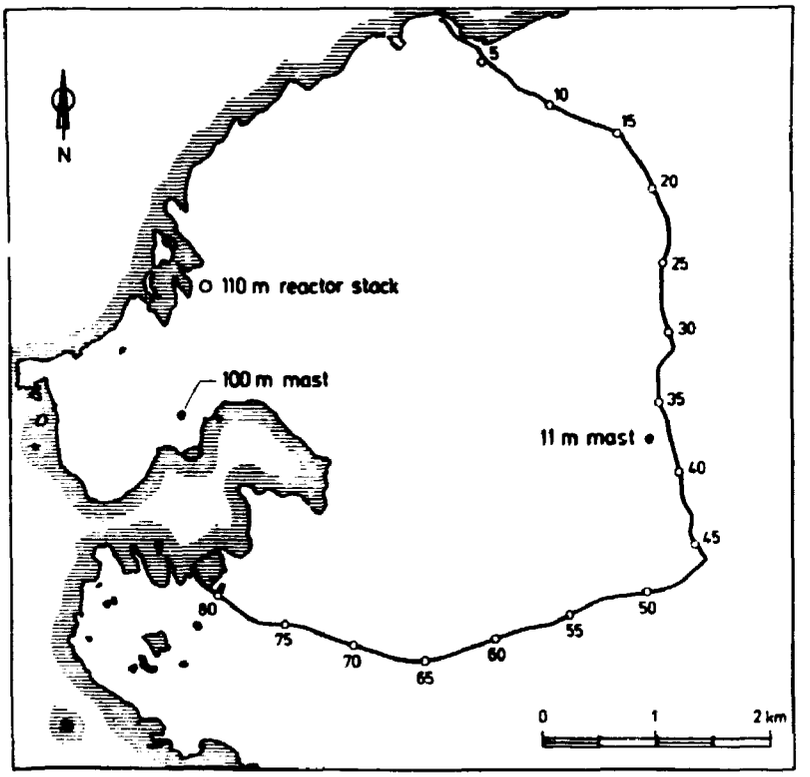

Fig.2. Map of the experimental site showing the location of the reactor stack, the two meteorological masts, and the measurement line with the 82 positions.

An 11-m meteorological mast was set up near the measurement line (see Fig. 2) giving information on the meteorological conditions.

The decision to initiate an experiment was based upon a good meteorological forecast. The wind direction should be persistent and towards land, which from the stack covers a sector of approximately 130°. The setting-up of the sampling network

required one hour. The network covered an angle of approximately 40° as seen from the power plant and was located with the center at the expected centerline of the plume. This centerline was found from the mean wind direction and was verified from several traverses made by car along the measurement line with sensitive scintillation detectors.

3.1. Meteorological measurements

3.1.1. Instrumentation

The purpose of the meteorological measurements during the campaign was partly to obtain information of the local windfield that is needed in order to carry out the experiments, and partly to document the meteorological conditions at the site during the individual experiments. The meteorological measurements that were carried out during the campaign will be discussed below.

Ringhals Mast. A 100-m meteorological mast is permanently positioned close to the power plant, Fig. 2, located at the summit of a 15-m steep hill at a very undulating part of the peninsula. The mast is instrumented for routine measurements of wind speed (24, 48 and 96 m), direction (24 and 96 m) and temperature (2, 12, 24, 48, and 96 m). Wind speed and direction are obtained from cup anemometers and wind vanes, and temperature is measured by ventilated thermometers. The output from these instruments are continuously recorded on stripcharts at the control center of the power plant, and is also averaged over 1 hour and stored on magnetic tape. However, due to the very inhomogeneous surroundings, the measurements from this mast are unsuited to a detailed analysis of the local meteorological conditions during the individual experiments.

Väröbacka Mast. An 11-m mast was therefore erected for this campaign in order to measure the parameters that are necessary for a detailed analysis of the local meteorological conditions during the various experiments. Such measurements

ideally should be carried out over a completely homogeneous area, and we put much effort in finding a suitable position for the mast. It was decided to place the mast at Väröbacka railway station, Fig. 2. Here a fairly homogeneous upstream fetch of about 1.5 km exists. However, downstream of the mast the conditions are less ideal.

The instrumentation of the mast is shown in Fig. 3. The following meteorological parameters are measured:

- wind speed at 2.3 and 8.4 metres height,
- wind direction at 2.3 and 8.4 metres height,
- temperature at 2.0 and 8.0 metres height,
- temperature difference between 2.0 and 8.0 metres height.

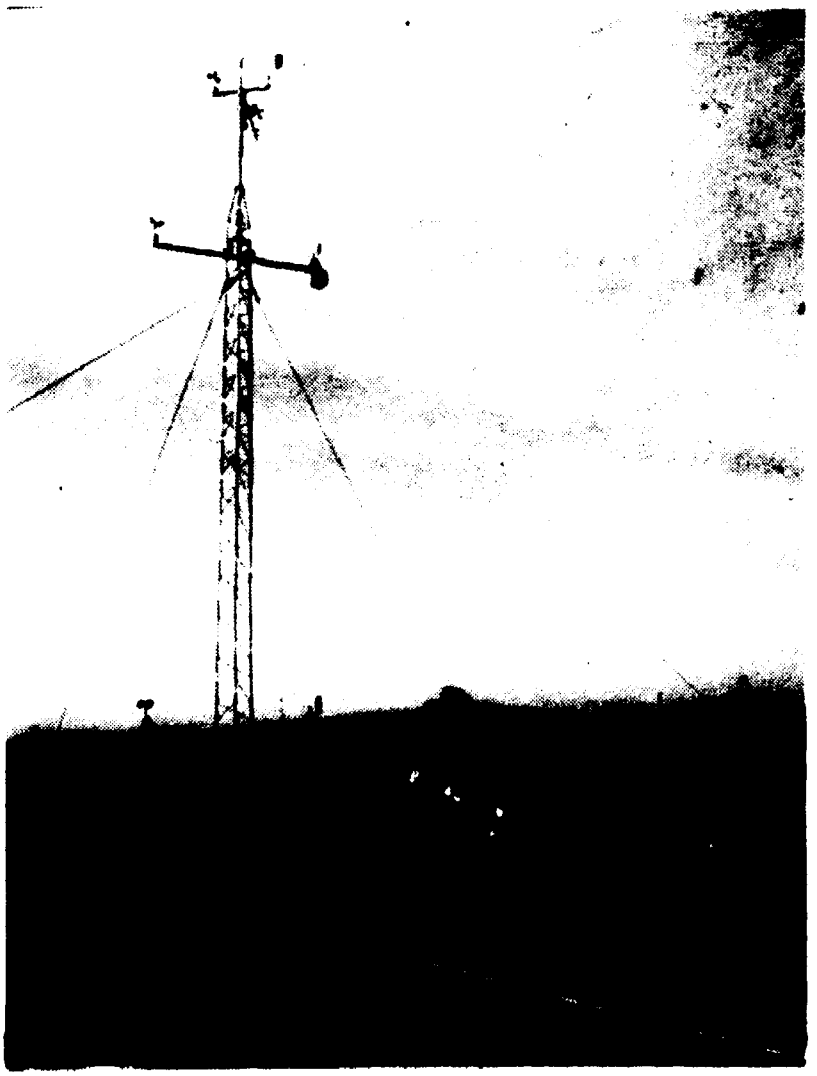

Fig.3. Instrumentation of the 11-m meteorological mast. Also shown is the radiosonde system.

These measurements are taken every 10 minutes, wind direction, temperature, and temperature difference are instantaneous values at the time of scanning, the wind speed is averaged over a period of 10 min. The registration is carried out by a datalogger with a mechanical scanner that reads the contents of 12 channels every 10 min; each reading of the channels takes about 1 min. The results are stored on magnetic tape.

Measurements of the wind speed are carried out with Risø-model 70 cup-anemometers that output two electric pulses per rotation of the cups. Wind direction is sensed by wind vanes of the potentiometer type and with oil-damped wind vanes manufactured by Aanderaa. Temperature is measured by platinum-resistance thermometers shielded in a screen of Risø design. The screen is ventilated by the wind alone.

In addition to the measurements every 10 min, measurements of the fluctuating wind velocity and fluctuating temperature were carried out during the experiments. The instruments for this was mounted on a boom at 11-m height; Fig. 4 shows the instrumented boom. The turbulence instrumentation is described in detail in Gryning and Thomson (1979) and Gryning (1981). A short description is given below.

A Risø-model 70 cup-anemometer is used as a wind-speed sensor. The distance constant is 1.5 m and the starting speed is 0.26 m/s. Wind direction is sensed using a light-weight vane also developed at Risø. The vane's natural wavelength is 1.5 m, and its damping ratio is 0.5. Vertical wind velocities are sensed using a helicord Gill-type propeller. However, the vertical velocities encountered during these experiments were so small that this vertical propeller was inappropriate for measuring these fluctuations, therefore, a description of this instrument is left out. Temperature fluctuations are derived from a single pair of copper-constantan thermocouples. The fluctuations are derived from the instantaneous temperature difference between a thermocouple junction extending 5 mm into the air stream and a reference junction imbedded in the center

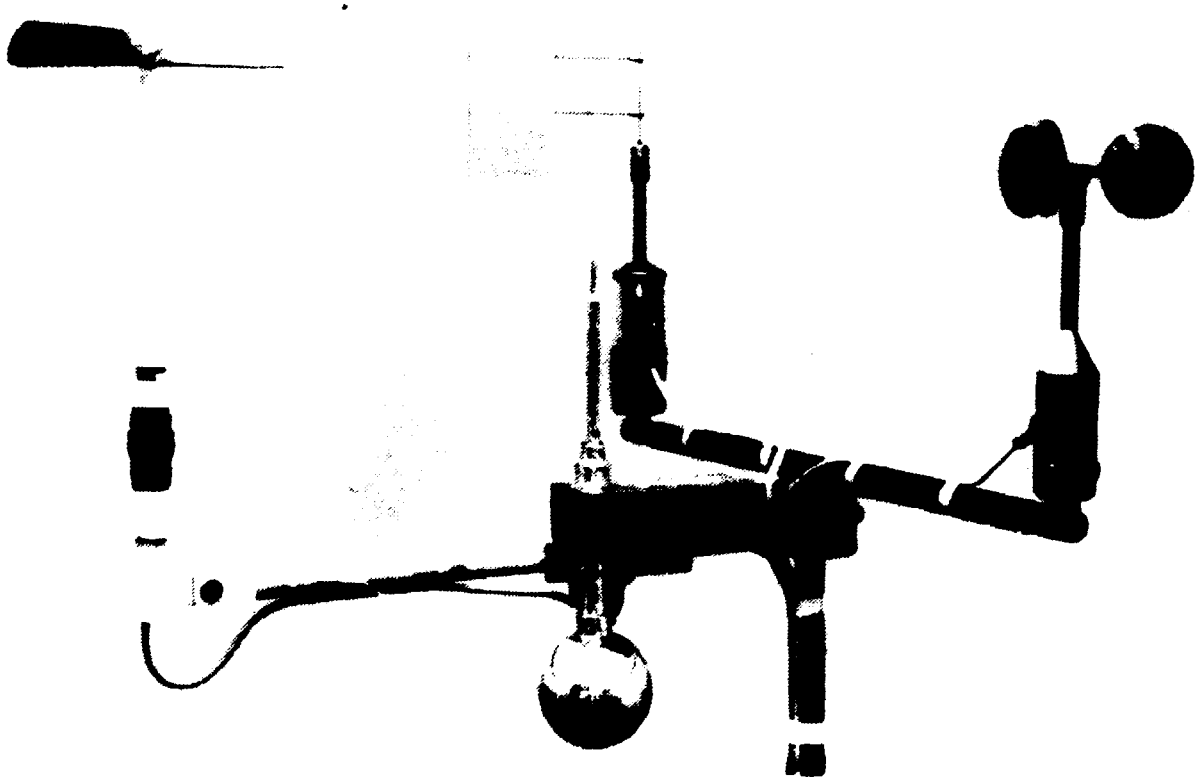

Fig.4. Turbulence-instrumented boom of the 11-m mast.

of a 10 cm acrylic sphere. (For a detailed description see Gryning and Thomson (1979).)

The analog or pulsed signals from these instruments were recorded continuously during the experiments on an FM-recorder, and were later digitised with a sampling frequency of 1 Hz.

During each experiment, a radiosonde that measures air pressure, air temperature, and wet-bulb temperature was launched near the small mast. This gives information on the vertical structure of temperature and humidity in the atmosphere. The sonde was flown with a free balloon in such a way that the ascent velocity was about 1.5 m/s. Data was transmitted from the sonde to a receiver on the ground every 3 s. On the ground the data were calibrated and then recorded in semi-digital form on a cassette-recorder, and later replayed into a computer for analysis.

3.1.2. Plume rise

The air that is released through the 110-m high ventilation stack has a vertical exit velocity of about 6.7 m/s and roughly a temperature of 31 °C. Due to the excess temperature the plume will tend to rise above the stack. However, wind blowing past a stack induces a wake on the lee side of it. If a plume is released with insufficient momentum and buoyancy it may be drawn into the wake and carried downward along the stack. This phenomenon is called downwash; it is likely to occur when $w_o/u<1.5$ where w_o is the gas exit velocity and u is the wind speed at the top of the stack. Values of w_o/u for these experiments are given in Table 1, it can be seen that downwash is likely to occur in the three daytime experiments.

Plume rise including downwash, near neutral conditions. The plume rise due to buoyancy will basically be calculated following the method that is devised in Hanna et al. (1982), the effect of downwash will be handled following the suggestions by Briggs (1981).

The calculations of the plume rise due to buoyancy will be based on the so-called break-up model; roughly speaking the final plume rise is assumed to occur when the entrained air has diluted the plume so much that the rate of eddy dissipation in the plume is the same as in the ambient air. Hanna et al. (1982) gives the formula for the final plume rise due to buoyancy, Δh_b, in near neutral conditions

$$\Delta h_b = 1.54 \left(\frac{F_o}{u u_*^2} \right)^{2/3} h_s^{1/3} \qquad (1)$$

where h_s is the stack height, u the wind velocity at the plume height, u_* the friction velocity, and F_o the initial buoyancy flux, defined as

$$F_o = 0.25 \frac{g}{T_p} \Delta t \, w_o \, D_i^2$$

with T_p being the absolute temperature of the plume; Δt is the excess temperature of the plume and D_i is the inner stack diameter.

Table 1. Characteristic plume-rise parameters for the experiments.

Experiment	conditions at stack top			experiments during: near neutral conditions			experiments during: stable conditions		
	u [1] (m/s)	w_o/u	T [2] (°C)	Δh_b (m)	Δh_d (m)	$0.25(D_o\ x_*)^{1/2}$ (m)	s [3] (s^{-2})	Δh_s (m)	Δh_{eff} (m)
I, May 23	8.4	0.8	11.5	39.3	-6.1	10.5			29
II, May 23-24	3.4	2.0	12.1				$1.4.10^{-4}$	89.1	89
III, May 25	7.9	0.8	10.7	47.7	-5.7	10.6			37
IV, May 28	13.5	0.5	12.6	18.8	-8.8	10.3			9

Inner stack diameter: 4.4 m, outer stack diameter: 5.0 m, stack height: 110 m, exit gas velocity: 6.7 m/s, gas temperature at stack top: 31 °C.

1) Extrapolated from measurements at the Väröbacka mast.

2) Based on the Ringhals-mast data, temperature at 96 m.

3) Based on the Ringhals-mast data, temperature difference taken between 96 m and 2 m.

There is very litte guidance available on calculations of plume rise under downdraft conditions. For a jet without buoyancy the downdraft, Δh_d, traditionally (Hanna et al., 1982) is given as

$$\Delta h_d = 2(w_o/u-1.5)D_i \qquad (2)$$

For buoyant plumes this simple correction may be inadequate, because plumes tend to interact with the stack wake for a long distance downwind, causing increased entrainment of air. Briggs (1981) suggests that this effect can simply be accounted for by subtracting from the plume rise formula "some fraction" of the width of the stack wake. The plume wake grows as $(D_o x)^{1/2}$ where D_o is the outer stack diameter and x is downward distance. We chose to subtract $0.25(D_o x_*)^{1/2}$ from the plume rise that could be

$$x_* = 6.49\ F_o^{2/5}(h_s + \Delta h_d)^{3/5},$$

which is partly based on Briggs (1969). The effective plume rise, Δh_{eff} in near neutral conditions are calculated in these experiments as

$$\Delta h_{eff} = 1.54 \left(\frac{F_o}{uu_*^2}\right)^{2/3}(110 + \Delta h_d)^{1/3} - 0.25\ (D_o x_*)^{1/2}, \quad (3)$$

and consequently, the effective stack height, h_{eff}, is

$$h_{eff} = h_s + \Delta h_{eff}$$

Plume rise, stable conditions. At night a stable layer forms near the ground at the same time as the wind speed decreases. The plume rise due to buoyancy under these conditions is controlled by the stability of the ambient air and consequently depends on other factors than those during daytime. Downdraft is not likely to occur during stable conditions due to the associated low wind velocities. The final rise of a plume during stable conditions, Δh_s, are given in Hanna et al. (1982):

$$\Delta h_s = 2.6 \left(\frac{F_o}{us}\right)^{1/3}, \qquad (4)$$

where s is a measure of the atmosphere stability

$$s = \frac{g}{T}\left(\frac{\partial T}{\partial z} + \Gamma\right).$$

Here Γ is the dry adiabatic lapse rate. According to Hanna et al. (1982) formulas for the final rise of jets in a stable atmosphere are not satisfactorily developed, the jet effect is believed to be small in the present case anyway, and will not be taken into account. Therefore, we set $\Delta h_{eff} = \Delta h_s$.

Plume rise at these experiments. The plume rises for the daytime experiments on May 23, 25 and 28 were calculated from (3), and the results together with some characteristic parameters are shown in Table 1. The plume rise in the experiment on the night May 23-24 is calculated from (4), however the wind speed at Väröbacka was close to the starting speed of the cup-anemometer, and therefore rather uncertain. The wind speed at the plume height was therefore taken as the measured 96-m wind speed at the Ringhals meteorology mast.

Table 2. Effective stack heights and the wind speeds at these heights. Also shown is the uncertainty on the plume rise calculated by increasing/decreasing Δh_{eff} by 40%.

	Δh_{eff} decreased by 40%		Δh_{eff} unaltered		Δh_{eff} increased by 40%	
Experiment	h_{eff} (m)	$u(h_{eff})$ (m/s)	h_{eff} (m)	$u(h_{eff})$ (m/s)	h_{eff} (m)	$u(h_{eff})$ (m/s)
I May 23	127	8.4	139	8.5	151	8.5
II May 23-24	163	3.5	199	3.5	235	3.5
III May 25	132	8.0	147	8.0	162	8.0
IV May 28	115	13.5	119	13.6	123	13.6

The uncertainty on Δh_{eff} is generally believed to be about 40%. Table 2 shows effective stack heights and associated wind-speeds for Δh_{eff} increased/decreased by 40% and for Δh_{eff} unaltered.

3.1.3. Meteorological conditions

The measurement results at the meteorology mast at Väröbacka railway station were used for the calculation of the Monin-Obukhov length L, which is a measure of the atmospheric stability, the friction velocity u*, which is a characteristic velocity, and the roughness length z_o, which is a characteristic length for the surrounding area. As the insolation, wind speed and wind direction vary from experiment to experiment, L, u* and z_o will vary also.

The Monin-Obukhov stability length was determined following a method that was devised by Golder (1972). First, we introduce the gradient Richardson number, which is defined as

$$Ri = \frac{g}{T} \frac{\partial\theta/\partial z}{(\partial u/\partial z)^2} \qquad (5)$$

where g is the gravity, T is the absolute temperature, θ is the potential temperature, u is the wind-speed and z the height.

In practice, however, it is very difficult to measure $\partial u/\partial z$. In order to overcome this the so-called bulk Richardson number is introduced:

$$B = \frac{g}{T} \frac{\partial\theta/\partial z}{u^2} z^2 \qquad (6)$$

In these experiments the potential temperature gradient is approximated by the mean temperature gradient between 2 and 8 metres height

$$\frac{\partial\theta}{\partial z} = \frac{T_8 - T_2}{8-2} + \Gamma$$

with Γ , the dry adiabatic lapse rate set equal to $0.98 \cdot 10^{-2}$ (^{o}C/m). The wind speed u in (6) pertains to the height

$$z_m = (z_1\ z_2)^{1/2},$$

where z_1 and z_2 are the heights for the measurements of temperatures. It can easily be seen by comparing (5) and (6) that the bulk Richardson number is related to the Richardson number through

$$Ri = B \frac{u^2}{\{\partial u/\partial(\ln z)\}^2} \qquad (7)$$

In order to eliminate the wind-speed from the above expression we introduce the dimensionless wind-shear, ϕ_m.
Monin-Obukhov similarity theory postulates that ϕ_m is a function of the Richardson number only

$$\phi_m(Ri) = \frac{\kappa z}{u_*} \frac{\partial u}{\partial z} \qquad (8)$$

where κ is the von Kármán constant. Integration of (8) leads to the expression for the wind profile

$$u = \frac{u_*}{\kappa} \{ \ln(z/z_o) - \psi(Ri) \} \qquad (9)$$

where z_o is the momentum roughness length and ψ is another function of Ri. Elimination of u by inserting (8) and (9) in (7) leads to

$$Ri = B \left\{ \frac{\ln(z/z_o) - \psi(Ri)}{\phi_m(Ri)} \right\}^2 \qquad (10)$$

A number of empirical expressions for ϕ_m (and consequently of ψ) have been suggested in the literature. We used Dyer's (1974) expressions for unstable and neutral conditions

$$\phi_m(Ri) = (1 - 16\ Ri)^{-0.25}$$

and

$$\psi(Ri) = 2\ \ln[(1+x)/2] + \ln[(1+x^2)/2] - 2\ \mathrm{Arctan}(x) + \pi/2$$

with

$$x = \phi_m^{-1}(Ri) \qquad \text{and } Ri = z/L.$$

We did not apply this technique for estimating L under stable conditions, consequently the corresponding expressions for stable conditions are omitted.

Knowing the wind-speed at heights z_1 and z_2, then the friction velocity can be estimated from the wind profile expression. This leads to

$$u_* = \frac{\kappa\,(u(z_1)-u(z_2))}{\ln z_1 - \ln z_2 - \psi(z_1/L) + \psi(z_2/L)} \qquad (11)$$

The roughness length can be calculated in a similar way:

$$z_0 = \exp\left\{ \frac{1}{\frac{u_1}{u_2} - 1} \left[\{\ln z_2 - \psi(z_2/L)\} - \ln z_1 + \psi(z_1/L) \right] \right\} \qquad (12)$$

In practice we estimate L, u_* and z_0 by an iterative procedure. First a value of L is guessed. Using this L value u_* and z_0 are calculated from (11) and (12). With the new estimates for u_* and z_0 the wind-speed at the height z_m is calculated. Then B is calculated using the measured values of $\partial\theta/\partial z$, estimated value for $u(z_m)$, and knowing B, Ri is calculated from (7); finally L is calculated as $L = z_m/Ri$ and this value of L is compared to the estimated L-value. This iteration process is continued until agreement between the guessed and the calculated L values are obtained. Then final values of u and z_0 are calculated, and this allows us to calculate the wind-speed at any height within the surface layer by (9).

Table 3. Meteorological conditions during the experiments.

Experiment	Ringhals mast	Väröbacka mast								Pasquill (1961)
	u 96 m (m/s)	u 10 m (m/s)	σ_v 11 m (m/s)	T 2 m (°C)	$\Delta T/\Delta z$ (2-8 m) (°C/m)	u_* (m/s)	L (m)	z_o (m)	z_i (m)	stability class
I, May 23 1431-1531	8.0	6.7	0.95	14	-0.16	0.44	-44	0.03	400	D
II, May 23-24 2324-0024	3.5	nd	nd	10	0.10	nd	nd	nd	nd	Stable (E) [1]
III, May 25 1133-1233	6.9	6.4	1.1	13	-0.14	0.40	-40	0.02	600	D
IV, May 28 1240-1340	13.8	10.8	1.1	15	-0.11	0.58	-137	0.01	900	D

nd - not possible to determine

[1]) Subjectively determined

Table 3 shows the meteorological parameters for the 4 experiments. The standard deviation of the lateral wind velocity, σ_v, is derived from the measurements that were performed with the turbulence instruments. The inversion heights were estimated from the radiosonde launches that were carried out at the Väröbacka mast. Figure 5 shows a recorded temperature profile from the radiosonde launched during experiment I indicating an inversion at about 400 metres height.

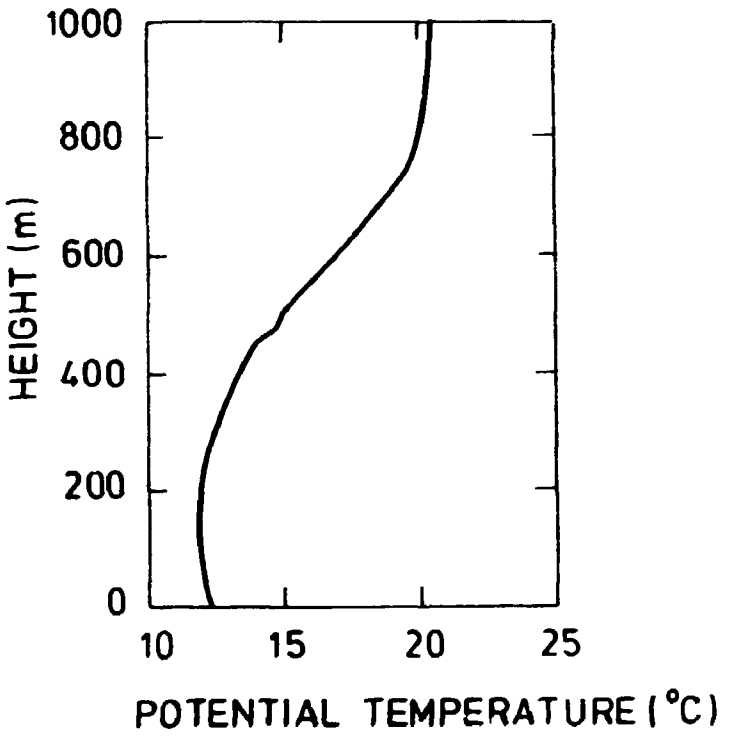

Fig.5. Temperature profile from the radiosonde launched during experiment I indicating an inversion at about 400 metres height. Neutral conditions are indicated by a constant potential temperature and stable conditions are indicated by an increasing potential temperature as a function of height.

3.2 SF_6-tracer measurements

The tracer, sulphurhexafluoride, SF_6, is a chemical inert and non-toxic gas. There are no natural and only few and small man-made sources. The background concentration of SF_6 is very low ($< 10^{-12}$ parts per part).

3.2.1 Tracer release system

In the actual experiments SF_6 was released to the atmosphere together with the stack gas effluent.

The tracer SF_6 is available in cylinders. For these experiments 3 cylinders each containing 41.6 kg of SF_6 were placed in the reactor building.

The release flow system consisted of a pressure reduction constant flow regulator, a flowmeter and a nylon pipe connected to a flange in the noble gas monitoring system. A constant tracer release rate was verified by observing the flowmeter. The rate of release, shown in Table 4, was calculated from the weight of the cylinders before and after an experiment and the duration of the release. Also shown in the table are the release times.

The time interval from start of tracer release to start of the one-hour sampling was long enough to ensure that the tracer had been transported and spread fully in the sampling area. From the windspeed u, (Table 2) and the actual downwind distance to the sampling area, x, this time interval can be seen to range from 2 to 4 times x/u. The release was stopped when the sampling stopped.

The accuracy of the release rate is estimated to be better than 4%. The time variation of the release rate during an experiment is within a few per cent.

3.2.2. Tracer sampling equipment

Automatic radio-controlled air-sampling units, based on sampling in plastic bags, were used. Figure 6 shows the interior of a unit. Air is sucked in through an intake tube by a small diaphragm pump and let in to one of three plastic bags which are inflated with a flow rate of about 300 ml/min; the inflation of the bags is regulated by magnetic valves. The units inflate the three plastic bags in sequence, each having a sampling time of 20 min. The sampling procedure is started by coded

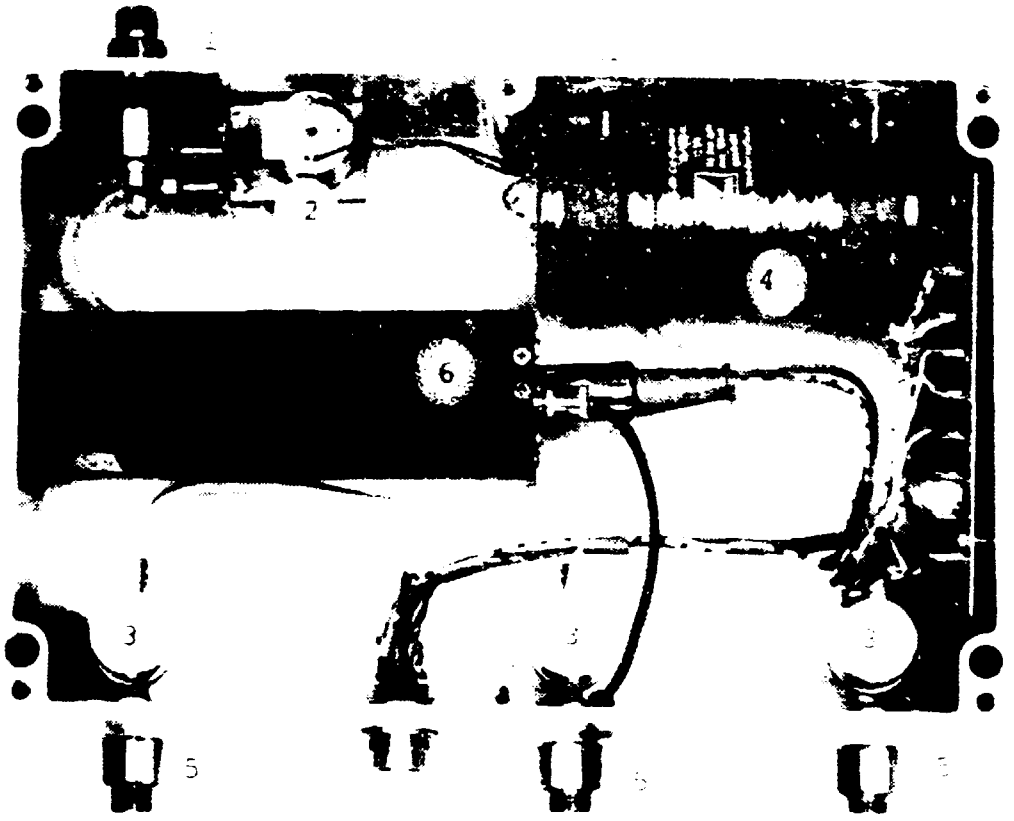

Fig.6. Interior of radio-controlled SF_6-tracer sampling unit. 1) fitting for mounting of the intake tube, 2) diaphragm pump, 3) magnetic valves, 4) NiCd batteries, 5) fittings for mounting of the plastic bags, 6) radio receiver for the start of the sampling.

signals to a radio-receiver in each unit. The power to the units is supplied by a battery in each unit that was recharged after each experiment. A total number of 40 units were used.

The signals to start sampling by the units were transmitted from a 6-watt transmitter positioned at the Väröbacka meteorological mast (Fig. 2). An antenna was mounted at the top of the mast (Fig. 3). The radios were operated at a frequency of 447.150 MHz; the signals were always properly received by the sampling-units.

Together with the tracer analysis equipment the tracer-sampling-units were installed in a laboratory at the Ringhals power

plant. Here the units were held stand-by for the experiments. Standby procedures included securing the proper rechargement of the batteries, checking the sampling flow rates and the functions of the radio-receivers.

Table 4. SF_6-tracer-release data

Experiment	Start of release (hrs)	Stop of release (hrs)	Release rate (g/s)	flowmeter (%)
I, May 23	1350	1530	3.17	40
II, May 23-24	2215	0023	2.33	30
III, May 25	1055	1235	2.30	30
IV, May 28	1212	1342	4.78	50

3.2.3 Tracer analysis

All air samples were brought to the power plant area after each experiment and analysed for their content of sulphurhexafluoride. The tracer concentrations were measured by means of a pulsed electron capture detector gas chromatograph equipped with a molecular sieve column. The gas chromatograph was calibrated by means of tracer standards prepared in advance of the experimental campaign. The detection limit was about 6 ng/m^3 with a signal-to-noise ratio of about 2. The tracer concentration in these standards is believed to be known with an uncertainty of 20%. This uncertainty leads to a systematic error that influences all concentrations identically during the experimental campaign. The reproducibility of the tracer standards within the time necessary to analyse the samples from one experiment was about 4%; This uncertainty affects the measured concentrations randomly. After the analysis the plastic bags were flushed with filtered air and reused.

3.2.4 Results of the tracer measurements

The tracer sampling units were positioned on a crosswind line according to the actual and a forecasted wind direction about 1 hour before the sampling period. The intention with the set-up of the units was to measure a full tracer plume in detail, corresponding to a separation between the observations of about 1.5 degrees as seen from the release position.

In experiment II, May 23-24, the concentrations for all samples at positions 46 to 78, Fig. 2, were near or below the detection limit and no plume structure could be found. Results from this experiment are not shown. Results from the three other experiments are given in Table 5 - 7. In experiment I, May 23, Table 5, the tracer plume is well covered by the tracer unit set-up. In the experiment III, May 25, Table 6, and especially the experiment IV, May 28, Table 7, the plume is less well covered. In all three runs in both these experiments it seems, however, that the maximum concentration on the crosswind line have been measured. Furthermore, the shape of the measured crosswind concentration distribution indicates that the individual runs could simply be extrapolated to zero concentration as shown in the tables.

For the three successful experiments the runs are averaged to get 1-h-average-concentration distributions, Tables 5 - 7, to be used in further analysis and model simulation.

From the 1-h-average-concentration distribution a position - a "center of mass" - is found as the position in the measuring arc where the area below the concentration distribution is divided into two parts of equal areas. The wind-direction in Tables 5 - 7 is the direction from the release position to the center of mass. For drawings (Fig. 14 and 15) and analysis of the measured concentrations the measuring positions have been projected on a line through the center of mass and perpendicular to the wind direction defined above. The distances on this crosswind line between projected neighbouring positions are also shown in the tables.

Table 5. Measured SF_6-tracer-concentrations and calculated mean concentrations at experiment I. Downwind distance 4100 m.

Position	Tracer-concentration (ng/m^3)				Distance*) (m)
	Run 1	Run 2	Run 3	Run 1-3	
48	0	0	0	0	
					145
49	13	0	0	4	
					121
50	40	10	0	17	
					117
51	78	40	0	39	
					121
52	331	219	0	183	
					129
53	901	1006	17	641	
					132
54	2885	2396	7	1763	
					132
55	3746	2497	51	2098	
					136
56	1569	3216	3679	2821	
					117
57	1873	3830	650	2118	
					118
58	769	3712	1544	2009	
					123
59	54	2177	2295	1509	
					121
60	27	1104	3544	1558	
					112
61	0	118	3189	1102	
					116
62	0	67	1016	361	
					130
63	0	0	273	91	
					115
64	0	0	0	0	
Sampling period	1431 -1451	1451 -1511	1511 -1531	1431 -1531	

*) Crosswind distance between neighbouring positions, wind-direction 312° (further explanation in the text).

Table 6. Measured SF_6-tracer-concentrations and calculated mean concentrations at experiment III. Downwind distance 3100 m.

Position	Tracer-concentration (ng/m^3)				Distance*) (m)
	Run 1	Run 2	Run 3	Run 1-3	
-1[1)]	0	0	0	0	
					40
0	170	90	328	196	
					57
1	805	139	372	439	
					123
2	1517	279	637	811	
					135
3	895	289	491	558	
					119
4	778	72	314	388	
					150
5	632	97	22	250	
					135
6	289	76	11	125	
					124
7	43	29	0	24	
					165
8	14	0	0	5	
					123
9	0	0	0	0	
Sampling period	1133 -1153	1153 -1213	1213 -1233	1133 -1233	

*) Crosswind distance between neighbouring positions, wind-direction 224° (further explanation in the text).

1) The concentrations in run 1, 2, and 3 have been extrapolated (see the text).

Table 7. Measured SF_6-tracer-concentrations and calculated mean concentrations at experiment IV. Downwind distance 3100 m.

Position	Tracer-concentration (ng/m^3)				Distance*) (m)
	Run 1	Run 2	Run 3	Run 1-3	
-2[1)]	0	0	0	0	
					79
-1	274	2344	4359	2326	
					39
0	340	2223	5696	2753	
					60
1	791	3838	6182	3604	
					124
2	2935	5523	5905	4787	
					135
3	5835	4863	2153	4284	
					121
4	4342	1329	285	1985	
					149
5	441	139	0	193	
					135
6	132	0	0	44	
					126
7	14	0	0	5	
					165
8	0	0	0	0	
Sampling period	1240 -1300	1300 -1320	1320 -1340	1240 -1340	

*) Crosswind distance between neighbouring positions, wind-direction 222° (further explanation in the text).

1) The concentrations in run 1, 2, and 3 have been extrapolated (see the text).

The lateral standard deviation of the tracer concentration distribution, $(\sigma_y)_{mea}$ is derived as the square root of the second moment of the tracer concentration distribution. It was calculated by means of the standard formula

$$(\sigma_y)^2_{mea} = \frac{\Sigma(\bar{\chi}_i\, y_i^2)}{\Sigma\bar{\chi}_i} - \left(\frac{\Sigma(\bar{\chi}_i\, y_i)}{\Sigma\chi_i}\right)^2$$

where $\bar{\chi}_i$ is the measured tracer concentration and y_i the corresponding crosswind distance. The crosswind-integrated concentration, $(\chi_{CWI})_{mea}$, was approximated by

$$(\bar{\chi}_{CWI})_{mea} = \frac{1}{2}\,\Sigma(\bar{\chi}_{i-1} + \bar{\chi}_i)\Delta y_i$$

where Δy_i is the crosswind distance between positions i-1 and i.

The standard deviation of the vertical tracer concentration distribution, $(\sigma_z)_{est}$, could be inferred only indirectly from continuity considerations, assuming a vertical Gaussian distribution. Assuming this, the crosswind-integrated tracer concentration at ground level can be expressed in terms of the effective height of release H_{eff} (Table 2), the transport velocity of the plume u (here taken as the mean wind speed at the height H_{eff}), the source strength of the tracer Q, and the vertical standard deviation, σ_z, as

$$\frac{u\chi_{CWI}}{Q} = \sqrt{\frac{2}{\pi}}\,\frac{1}{\sigma_z}\exp\left[-\frac{1}{2}\left(\frac{H_{eff}}{\sigma_z}\right)^2\right] \qquad (13)$$

which constitutes a relation between σ_z and the normalised crosswind-integrated concentration, $u\chi_{CWI}/Q$ for a given value of H_{eff}.

Reflection of the tracer at the height of inversion (Table 3) is not taken into account because the effect is negligible in the present experiments. The right-hand side of equation 13 seen

as a function of σ_z for a given value of H_{eff} has a maximum for $\sigma_z=H_{eff}$. This means that if an observed value of $u\chi_{CWI}/Q$ is larger than the value of the right-hand side with $\sigma_z=H_{eff}$, no value of σ_z to fulfill equation 13 can be found. In these cases - experiments I and IV - we put $(\sigma_z)_{est}=H_{eff}$.

Values of $(\sigma_y)_{mea}$, $(\chi_{CWI})_{mea}$, and $(\sigma_z)_{est}$ for the experiments are given in Table 8. Also given in the table is the value of the right-hand side of eq. 13 with $\sigma_z=(\sigma_z)_{est}$ multiplied with the appropriate Q/u. These values are to compare with $(\chi_{CWI})_{mea}$. It is seen that the uncertainty of ± 20% on $(\chi_{CWI})_{mea}$ cannot account for the difference.

Table 8. Parameters calculated from the one-hour SF_6-tracer concentration distribution.

Experiment	$(\sigma_y)_{mea}$ (m)	$(\chi_{CWI})_{mea}$ ($\mu g/m^2$)	* ($\mu g/m^2$)	$(\sigma_z)_{est}$ (m)
I, May 23	299	2021	1310	139
II, May 23-24	-	-	-	-
III, May 25	200	332	332	68
IV, May 28	160	2072	1440	119

* Q/u multiplied by right-hand side of eq. 13.

3.3. Gamma-ray measurements

3.3.1. Noble gas source term

The noble gas leakage is ventilated through a 110-m stack and is measured with a monitoring system.

Samples of the stack air is taken through four inlets in the cross section of the stack, and the concentrations of the radioactive noble gases are determined from measurements made with a germanium detector connected to a multichannel analyser. Mean values of the concentration of the isotopes are printed out every hour.

During measurements reported in Karlberg et al., (1980) the accuracy of the monitoring system was tested. The total stack flow was measured with respect to magnitude and stability (Ström and Karlberg, 1980). The measured flow was 15% less than the nominal value and no significant time variation was found. The performance of the stack sampling method was also investigated in an ^{131}I-injection experiment and no significant bias was found.

Table 9. Noble-gas source terms for the experiments (MBq/s).

	Source terms (MBq/s) for the experiments			
Nuclide	I	II	III	IV
Kr85m	27.2	28.1	25.2	24.6
Kr 87	55.3	53.6	49.0	44.7
Kr88	62.5	63.3	57.5	54.6
Kr89	10.2	9.8	9.5	8.2
Xe133	38.3	42.7	37.1	39.9
Xe135	89.3	85.0	82.3	78.1
Xe131m	119	87.1	79.0	99.1
Xe135m	56.1	54.4	51.0	47.6
Xe137	28.1	29.3	27.4	26.3
Xe138	82.0	68.4	65.3	61.6

The release rates of the noble gases are given in Table 9 for the four experiments. Only release rates from the BWR stack are included. Contributions from other sources (eg. the PWR units) were negligible. The stack filtration system effectively removes particulates from the release including noble gas daughters (Aronsson, 1983).

3.3.2. Equipment

The instruments for field measurements of gamma rays from the plume comprised 11 Geiger-Müller counters, three ionisation chambers, and three gamma-spectrometer systems.

The GM counters were Environmental Radiation meters from Mini-instruments Ltd, UK. The GM tubes were of type MC70. Each instrument was contained in a carrying case with detector, scaler and a tripod. Output was available from an analog logarithmic display in units of μGy/h and from a digital display in counts integrated over a pre-selected period of time.

The ionisation chambers were from Reuter Stokes Inc., USA, and of the type RSS-111. The spherical chambers have a diameter of 25 cm and are filled with argon at a pressure of 25 atmospheres. For two of the chambers output was available on magnetic tape in digital form containing instantaneous values of the exposure rate in units of μR/h recorded every 5 s. The data on the tapes were processed later on a computer. For one of the chambers the analog linear output from a strip-chart recorder was used.

All chambers were equipped with mechanical counters of the total exposure over a time interval. These integrators were not used, however, due to their insufficient resolution of one μR.

The gamma-spectroscopy systems were carried in motor vehicles equipped for transport of the systems and for furnishing electrical power. Two systems used lithium-drifted germanium detectors and one used an intrinsic germanium detector. The detectors were all placed in cryostats looking upward. The efficiencies ranged from 10-22% for 1.33-MeV photons relative to

the efficiency of a 7.5 x 7.5 cm NaI (Tl) detector. The detector resolutions ranged from 1.8-2.5 keV. Two of the multichannel analyser systems, a Canberra 8100 (4k) and a Nuclear Data 66 (2k), stored the recorded gamma spectra on paper tape. These spectra were analysed later on a computer using peak-fitting methods. The remaining multichannel analyser system, a Nuclear Data 600 (4k), used an inherent simpler method for spectrum analysis and delivered on-line results.

3.3.3. Calibration

A joint calibration was performed for all radiation instruments used in the measurements. Two certified point sources from Amersham, a 150 MBq ^{137}Cs-source and a 36 MBq ^{60}Co-source were used as calibration sources. The outputs were certified in terms of exposure rates at 1-m distance.

For each of the two sources a series of measurements were made at different exposure rate levels. This was accomplished by taking instrument readings at different source-to-detector distances: 3, 4, 5, 7, and 10 m, keeping the source and the detectors 1 m above the ground. Ground scatter was accounted for from calculations using data on gamma-ray albedo for concrete. The exposure rate at a distance d is obtained from the deca - corrected certified exposure rate at 1 m, $\dot{X}_1$,:

$$\dot{X}_d = \dot{X}_1 \frac{1}{d^2} \exp(-\mu d) F B$$

where μ is the linear attenuation coefficient for air at the gamma-ray energy of the source photons, F is the correction for ground scatter, and B accounts for the build-up in air. This calibration technique has proved to be accurate and reliable (Bøtter-Jensen, 1982). The set-up is depicted in Fig. 7.

The 11 GM-counters were numbered and calibrated individually. The results are shown in Table 10. The uncertainties are standard deviations from multiple determinations. The counter responses were divided in three distinct groups for which mean values

were calculated. The results demonstrate the sympathetic variation of GM-counter response with gamma-ray energy. An additional empirical correction factor had to be applied since the radioactive noble gases and their daughters emit gamma rays with energies over a much wider range than covered by the calibration. The correction factor was found from direct comparison between the ionisation-chamber results and the GM-counter results.

Fig.7. Calibration of gamma-ray detectors.

The results of the calibration of the ionisation chambers are shown in Table 11. The variations with energy of the observed gamma-ray responses were not statistically significantly different for any of the instruments. This is in agreement with the reported gamma-ray energy responses of these ionisation chambers (De Campo et al., 1972). Furthermore, it is noted that the chambers measure correctly the exposure rate from newly formed radioactive noble gases, like those released from the Ringhals reactor stack, when calibrated correctly for typical background radiation (Beck, 1982). Newly formed radioactive noble gases and their daughters yield high-energy gamma radiation like the natural background radiation. If, however, the

Table 10. GM-counter gamma-ray responses determined from measurements of certified point sources (cps or. μR/h).

GM counter No.	^{60}Co-source (1.25 MeV) individual ± sd	group mean ± sd	^{137}Cs-source (0.66 MeV) individual ± sd	group mean ± sd
1	0.1742 ± 0.0022		0.1407 ± 0.0014	
2	0.1700 ± 0.0024	0.1725 ± 0.0009	0.1382 ± 0.0014	0.1409 ± 0.0006
4	0.1727 ± 0.0011		0.1416 ± 0.0007	
3	0.1851 ± 0.0009		0.1464 ± 0.0017	
7	0.1837 ± 0.0018	0.1837 ± 0.0005	0.1456 ± 0.0020	0.1455 ± 0.0010
8	0.1822 ± 0.0008		0.1450 ± 0.0020	
10	0.1854 ± 0.0017		0.1447 ± 0.0020	
5	0.1581 ± 0.0021		0.1311 ± 0.0017	
6	0.1594 ± 0.0014	0.1603 ± 0.0008	0.1324 ± 0.0015	0.1332 ± 0.0009
9	0.1612 ± 0.0013		0.1355 ± 0.0021	
11	0.1617 ± 0.0018		0.1354 ± 0.0019	

Table 11. Responses of ionisation chambers to gamma-rays determined from measurements of certified point sources (μR/h measured per μR/h calculated).

Ionisation chamber	^{60}Co	^{137}Cs	Mean
1	0.982 ± 0.010	0.977 ± 0.010	0.979 ± 0.007
2	0.972 ± 0.019	0.978 ± 0.009	0.977 ± 0.008
3	0.900 ± 0.037	0.850 ± 0.025	0.866 ± 0.021

Table 12. Gamma-ray fluence rates ($\gamma/cm^2/s$), from certified point sources, ^{137}Cs and ^{60}Co, measured at a distance of 10 m with germanium detectors. In parentheses are given the results relative to the nominal source data which are converted assuming that the outputs from the sources consist of primary gamma rays only.

Spectrometer	662 keV	1173 keV	1332 keV
1	8.47 ± 0.05 (0.90)	2.49 ± 0.03(0.92)	2.52 ± 0.03(0.92)
2	8.86 ± 0.13 (0.94)	2.58 ± 0.04(0.96)	2.63 ± 0.04(0.96)
3	10.75 (1.14)	2.77 (1.03)	2.99 (1.10)
Nominal data	9.45 (1)	2.70 (1)	2.73 (1)

gaseous releases are more than 12 hours old, the radiation may be dominated by xenon fission gases emitting low-energy radiation, in which case the limited low-energy response of the ionisation chambers may cause highly inaccurate results for these instruments.

Table 12 shows the results of the gamma-spectrometer calibration. Measurements were made at a 10-m distance only of the two calibration sources. For comparison the certified source data were converted to gamma-ray fluence rates. This was done assuming that the certification concerns primary gamma-rays only, which is not completely the case. The error thus introduced is estimated to be less than 10%.

Gamma spectroscopy. The interpretation of the gamma-ray spectra from the plume is based upon a well-established technique (Beck, 1972 and Gogolak, 1984) derived for the measurement of radionuclides in the soil.

The basis of the technique is the equation

$$\frac{N_f}{\Phi} = \frac{N_f}{N_r} \cdot \frac{N_r}{\Phi} ,$$

where N_f is the full-energy-peak count rate (counts per second) registered in the field for a certain gamma-ray energy. N_r is the full-energy-peak count rate (counts per second) registered during calibration from a reference position, and Φ is the primary gamma fluence rate (photons cm^{-2} s^{-1}) at the detector point.

N_f/N_r is the energy-dependent correction factor for angular dependence. Assuming a general cylinder symmetry, the factor is calculated according to

$$\frac{N_f}{N_r} = \frac{\int_0^{\pi/2} R(\theta) \frac{d\Phi}{d\theta} d\theta}{\int_0^{\pi/2} \frac{d\Phi}{d\theta} d\theta} ,$$

where θ is the angle between the incoming photon and vertical, $R(\theta)$ is the angular response of the detector, and $d\Phi/d\theta$ is the

differential uncollided gamma-fluence rate 1 m above ground. Since the field measurements were planned to take place within the plume, the semi-infinite cloud model was considered adequate for the angular distribution of the uncollided gamma rays, yielding for the differential fluence rate

$$\frac{d\phi}{d\theta} = \frac{S \cdot f}{2\mu} \sin\theta$$

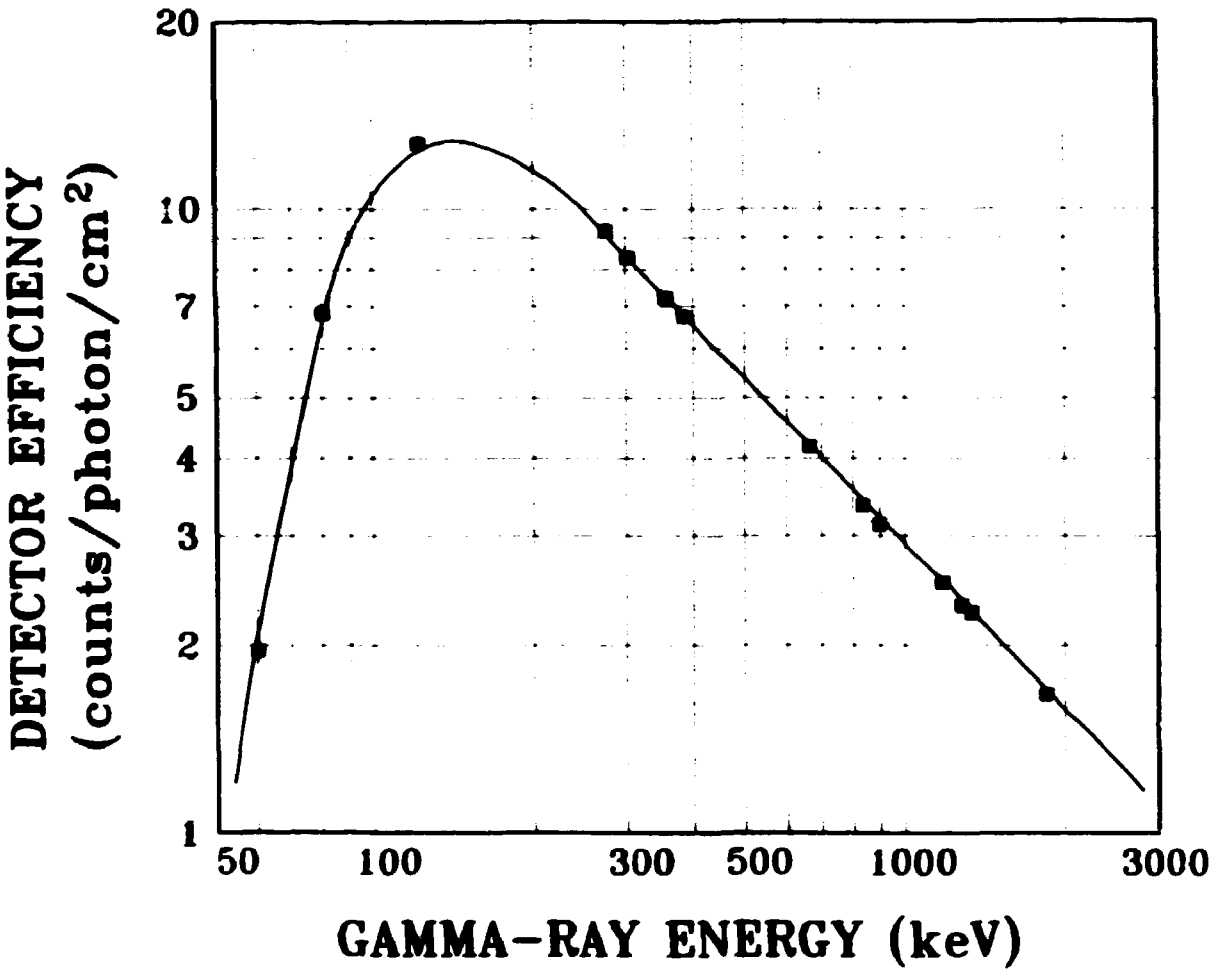

Fig.8. Germanium detector efficency (counts/photon/cm^2) versus gamma-ray energy (keV).

where S is the source concentration (Bq m^{-3}), f is the gamma yield (photons disintegration^{-1}), and μ the linear attenuation coefficient for air (m^{-1}).

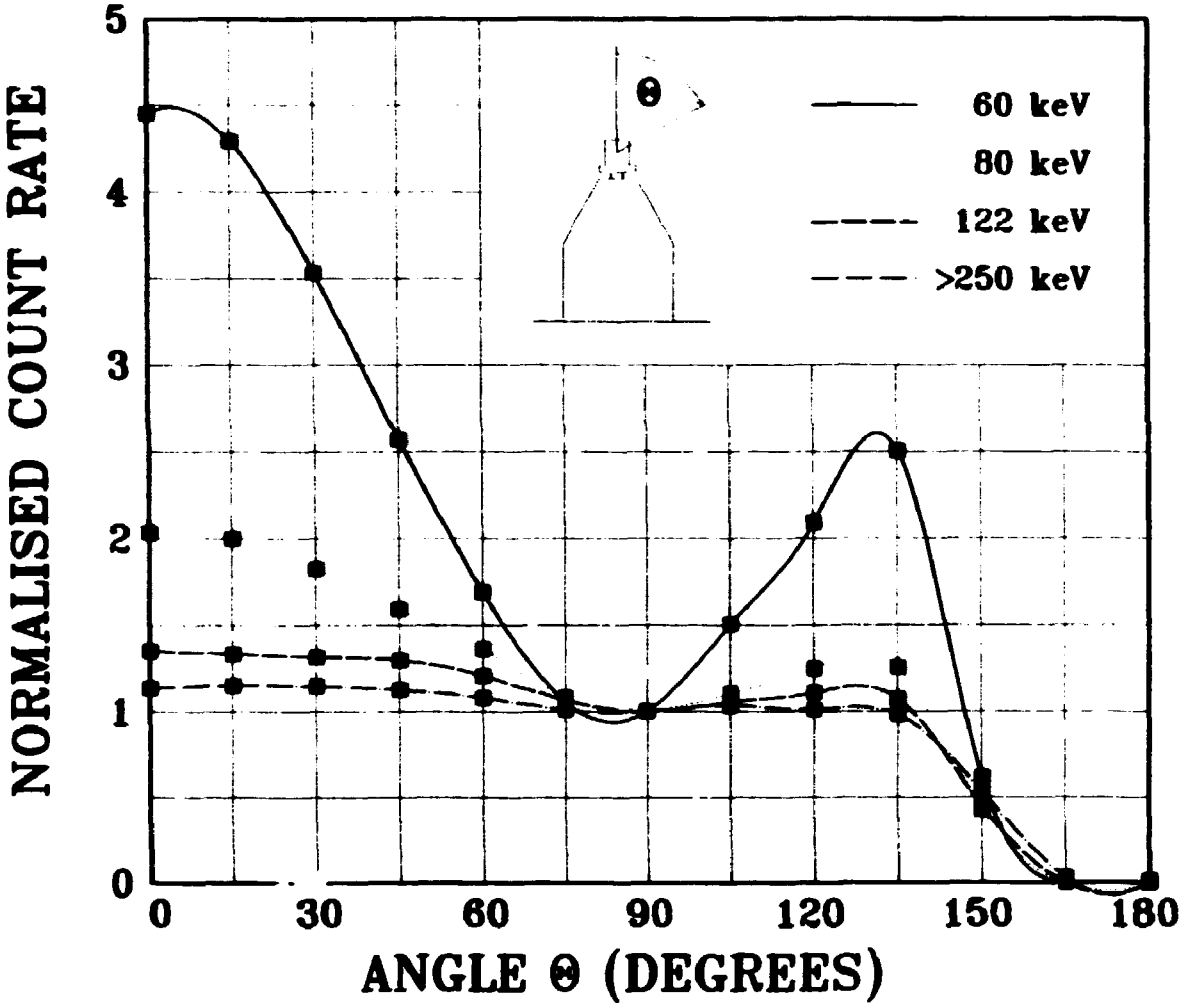

Fig.9. Relative angular response of a germanium detector for different gamma-ray energies.

N_r/ϕ is the detector efficiency (counts per photons cm^{-2}) determined by recording the full-energy-peak count rates from certified point sources placed sufficiently far from the detector to provide parallel beams over the detector volume.

The calibration of the gamma spectrometers with respect to efficiency and angular response was done in the laboratory, where the cylindrical symmetry of the detector responses was also verified. The results are shown for one of the germanium detectors. The efficiency, N_r/ϕ versus gamma energy, is shown in Fig. 8. The angular response $R(\theta)$ normalised to the response from the reference position is shown in Fig. 9, and the calculated angular correction factor N_ξ/N_r is shown in Fig. 10.

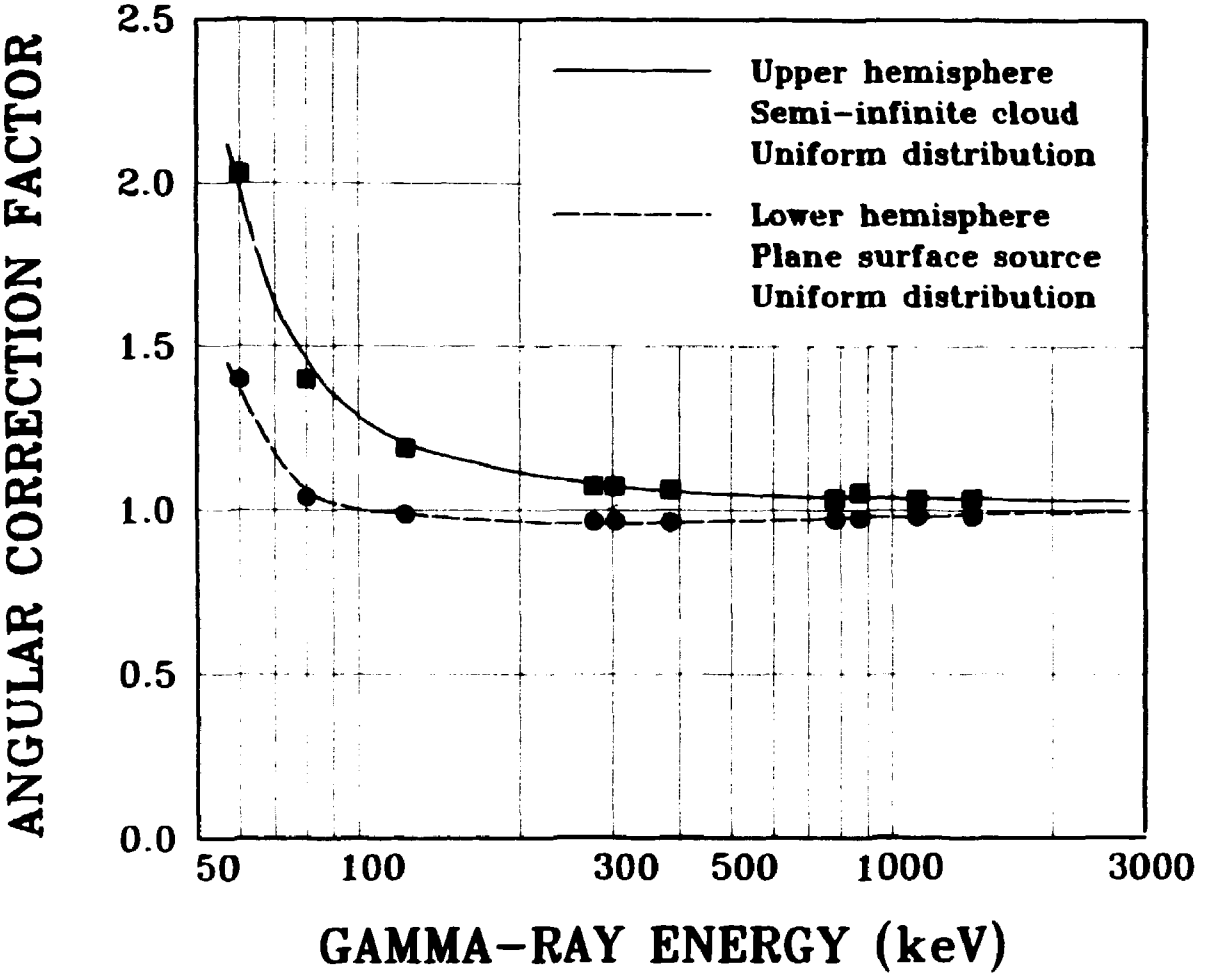

Fig.10. Calculated angular correction factors versus gamma-ray energy for a germanium detector. The factors are used to account for a homogeneous gamma-ray source distribution in the air or on the ground.

3.3.4. Results of radiation measurements

During each experiment the instruments were distributed along the measurement line in such a way as to achieve a full coverage of the plume profile. Due to the relatively few radiation instruments it was decided to place these at every second SF_6-sampling unit, thereby ensuring an average distance between the radiation instruments of about 300 m. Near the expected centerline of the plume three radiation monitoring stations were placed equipped with a GM-counter, an ionisation chamber, and a gamma spectrometer. The remaining GM-counters were distributed at either side of the centerline.

The location of the plume centerline was estimated from the mean wind direction and from short-term radiation measurements along the measurement line. But due to the obvious difficulties of locating the plume it was not possible until after each experiment to evaluate how fortunate the choice of measurement positions had been. The results of the radiation measurements from the GM-counters were readily available and yielded the first information on the plume location over the sampling period. Later this was compared with the results from the SF_6-sampling units when the SF_6-concentrations were determined in the laboratory by means of gas chromatography.

The problems with changes of wind direction during the sampling period are reflected in the varying instrumental coverage of the four experiments. Experiment I was the most successful considering that two measurement positions with ionisation chambers and gamma spectrometers were well within the plume. In experiments II and IV this was the case only for a single measurement position, and in experiment III for none.

Ionisation chambers and GM-counters. The results of the measurements with the ionisation chambers and the GM-counters are shown in Table 13. The table shows average net exposure rates ($\mu R\ h^{-1}$) at the measurement positions along the measurement line for the four experiments. Background readings to be subtracted from the experiment readings were obtained shortly after each experiment when the wind direction had changed sufficiently. Furthermore, the correct combination of measurement positions and instrument numbers was ensured for the background readings. Figure 11 shows details of the ionisation-chamber measurement in experiment I at position 55 as a function of time.

As seen from Table 13 the average exposure rates from the plumes were rather low compared to the background level of about 6 μR/h from the terrestrial component. In experiment III the levels may even not be significantly different from zero, but the indicated gamma profile coincides with the SF_6-concentration profile. Unfortunately, in this experiment a change of wind direction caused the measured profile to be based upon

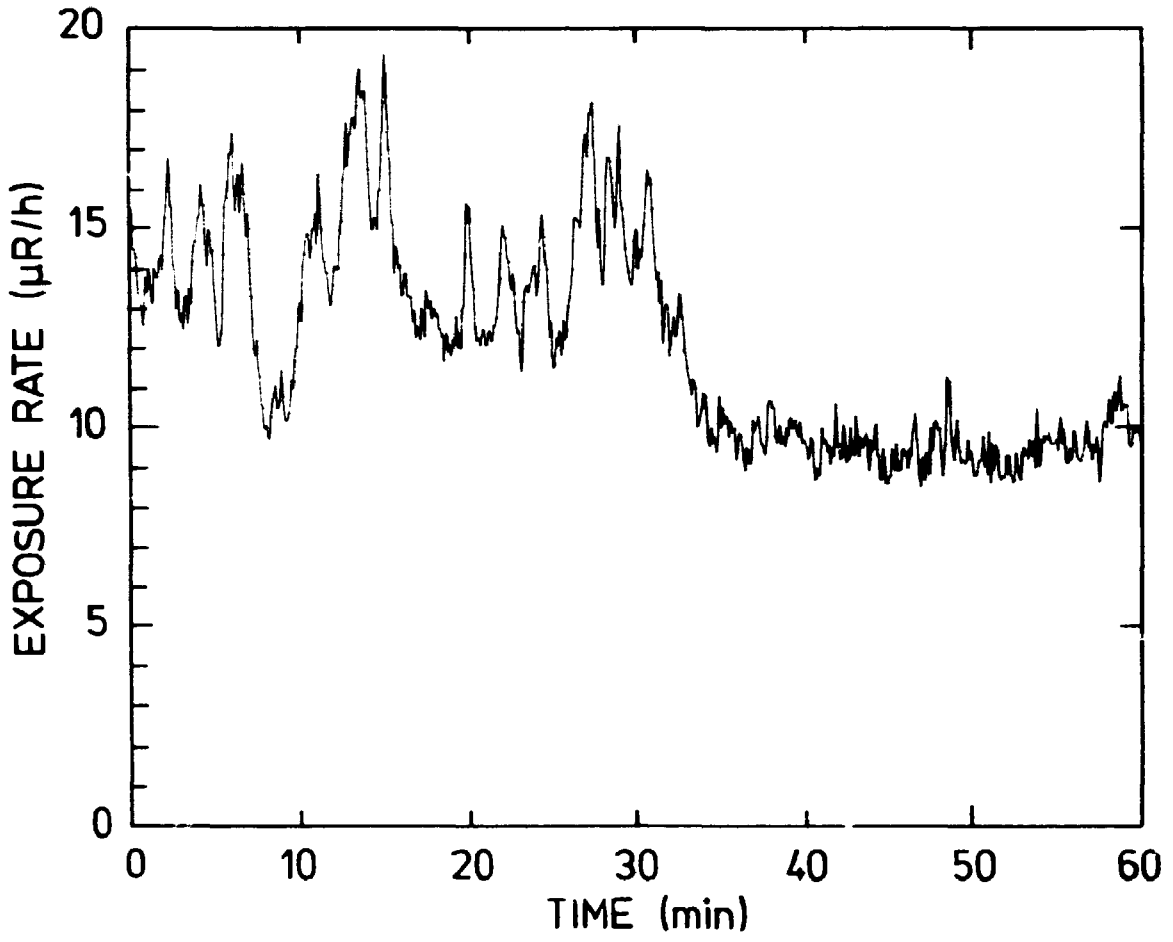

Fig.11. Ionisation-chamber measurement in experiment I at position 55. The radioactive plume appears to have been contributing the most during the first half of the one-hour measuring period.

GM-counters alone. The main part of the data in the table are from GM-counters, those from ionisation chambers are marked with an asterisk.

Problems with the evaluation of the GM-counter results were identified when the ionisation chamber results were evaluated. Based on either the ^{137}Cs- or the ^{60}Co-calibration the GM-counter results were much too high when compared with the ionisation chamber results. Since the ionisation chamber results were considered reliable, (cf. the discussion in Section 3.3.2) a general correction factor of 0.50 was applied to the GM-counter results converted with the individual sensitivities from the

Table 13. Net gamma-ray exposure rates from releases of radioactive noble gases at the experiments measured with GM-counters and ionisation chambers. The exposure rates are averaged over one hour. The measurement positions refer to locations shown in Fig. 2.

Experiment							
I		II		III		IV	
pos.	μR/h	pos.	μR/h	pos.	μR/h	pos.	μR/h
51	0.0*	68	0.0	1	0.4	-1	1.7
53	1.9	70	0.3*	3	0.6	1	2.9
55	3.1*	72	0.9	5	0.3	3	3.1
57	3.1	74	2.1	7	0.2	4	2.4*
59	3.7*	76	1.5	8	0.1	6	0.2
61	1.9	78	1.6	9	0.0*	7	0.1*
63	0.6	80	1.2			8	0.0
65	0.0	82	0.8				

* ionisation chamber results

^{60}Co calibration shown in Table 10. This general correction factor of 0.50 ± 0.02 was derived from the measurement at position 55 in experiment I and was supported from similar but less precise measurements at the other experiments.

Gamma spectrometers. The results of the gamma-spectrometer measurements during the experiments are shown in Tables 14 - 16. As mentioned previously there are no gamma-spectrometric results from experiment III due to an unexpected change of wind direction and in experiment II the results are too meager to be of use.

Table 14. Unscattered gamma-ray fluence rates, ϕ, (averaged over one hour) from radioactive noble gases and their daughters at experiment I measured at position 55.

Energy (keV)	Isotope	N_f (cps)	N_f/N_r	N_r/ϕ (counts γ^{-1} cm^{-2});	ϕ (γ m^{-2} s^{-1})
403	Kr87	0.374 ± 5%	1.05	6.48	550 ± 29
845	-	0.037 ± 20%	1.04	3.37	106 ± 21
2012	-	0.010 ± 20%	1.03	1.57	62 ± 12
2555 – 2558	-	0.033 ± 11%	1.03	1.42	222 ± 24
166	Kr88	0.104 ± 50%	1.14	12.5	73 ± 36
196	-	0.322 ± 6%	1.11	11.6	250 ± 14
835	-	0.077 ± 15%	1.04	3.41	218 ± 33
1530	-	0.030 ± 13%	1.03	1.99	144 ± 19
2030	-	0.014 ± 14%	1.03	1.55	90 ± 13
2035	-	0.017 ± 13%	1.03	1.55	105 ± 14
2196	-	0.046 ± 8%	1.03	1.45	309 ± 25
2392	-	0.106 ± 5%	1.03	1.34	768 ± 39
898	Rb88	0.070 ± 12%	1.04	3.19	210 ± 25
1836	-	0.064 ± 7%	1.03	1.70	366 ± 24
151	Kr85m	0.357 ± 5%	1.15	12.7	244 ± 11
305	-	0.060 ± 27%	1.07	8.31	68 ± 18
81	Xe133	0.210 ± 11%	1.40	6.7	224 ± 25
250	Xe135	1.696 ± 2%	1.08	9.88	1589 ± 21
527	Xe135m	0.371 ± 4%	1.05	5.11	691 ± 28
154	Xe138	0.067 ± 23%	1.15	12.7	46 ± 10
258	-	0.373 ± 5%	1.08	9.61	359 ± 18
435	-	0.154 ± 7%	1.05	6.06	242 ± 16
1768	-	0.074 ± 9%	1.03	1.76	407 ± 37
2005	-	0.020 ± 17%	1.03	1.57	122 ± 21
2016	-	0.044 ± 13%	1.03	1.56	276 ± 36
2252	-	0.005 ± 62%	1.03	1.42	34 ± 21
409	Cs138	0.047 ± 30%	1.05	6.39	70 ± 21
463	-	0.189 ± 6%	1.05	5.73	314 ± 18
547	-	0.075 ± 12%	1.05	4.94	144 ± 17
1010	-	0.089 ± 10%	1.04	2.88	297 ± 29
1436	-	0.196 ± 5%	1.03	2.11	902 ± 46
2218	-	0.029 ± 12%	1.03	1.44	197 ± 24
2640	-	0.013 ± 15%	1.03	1.23	99 ± 15

uncertainties (1 sd) from counting statistics only

Table 15. Unscattered gamma-ray fluence rates, Φ, (averaged over one hour) from radioactive noble gases and their daughters at experiment I measured at position 59.

Energy (keV)	Isotope	N_f (cps)	N_f/N_r	N_r/Φ (counts γ^{-1} cm^{-2})	Φ (γ m^{-2} s^{-1})
151	Kr85m	0.263 ± 19%	1.03	8.91	287 ± 54
403	Kr87	0.183 ± 9%	1.03	4.00	444 ± 40
196	Kr88	0.248 ± 14%	1.03	8.10	297 ± 42
250	Xe135	1.094 ± 5%	1.03	6.72	1580 ± 85
527	Xe135m	0.235 ± 10%	1.03	2.92	782 ± 76
258	Xe138	0.229 ± 16%	1.03	6.51	342 ± 55
435	-	0.106 ± 16%	1.03	3.65	281 ± 45
2016	-	0.022 ± 24%	1.03	1.09	195 ± 47
463	Cs138	0.128 ± 12%	1.03	3.39	366 ± 44
1010	-	0.047 ± 20%	1.03	1.53	299 ± 60
1436	-	0.089 ± 12%	1.03	1.23	699 ± 84

uncertainties (1 sd) from counting statistics only

The tables show the results sorted according to isotope. N_f is the photopeak count rate averaged over the measuring period of one hour, and the uncertainty is one standard deviation due to counting statistics only. N_f/N_r is the angular correction factor and N_r/Φ is the detector efficiency; these are explained in Section 3.3.3.

Figure 12 shows the gamma spectrum recorded in experiment I at position 55.

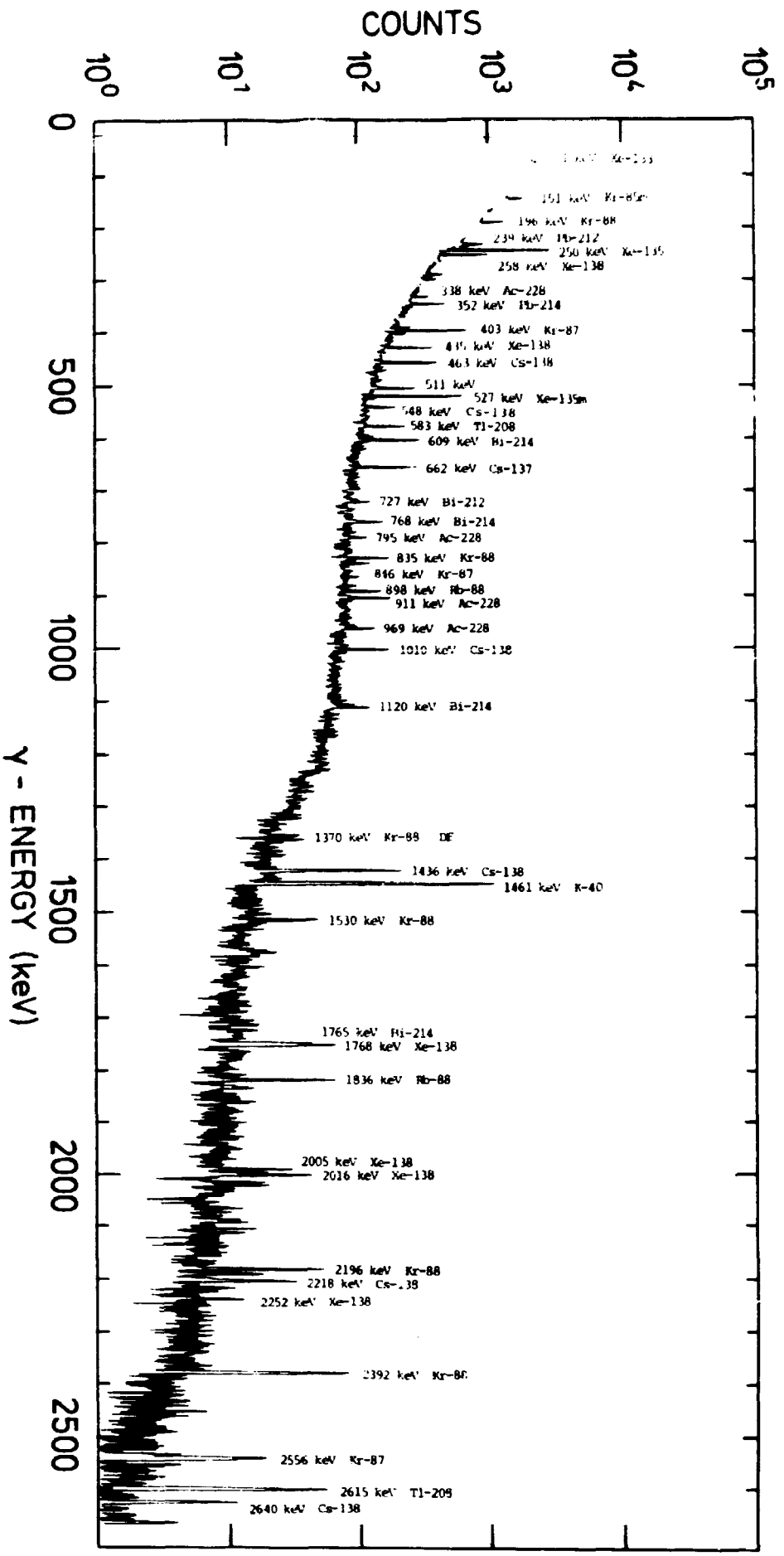

Fig.12. Gamma spectrum measured in experiment i at position 55.

Table 16. Unscattered gamma-ray fluence rates, ϕ, (averaged over one hour) from radioactive noble gases and their daughters at experiment IV measured at position 4.

Energy (keV)	Isotope	N_f (cps)	N_f/N_r	N_r/ϕ (counts γ^{-1} cm^{-2})	ϕ (γ m^{-2} s^{-1})
151	Kr85m	0.236 ± 17%	1.14	11	188 ± 32
305	-	0.058 ± 29%	1.09	6.35	84 ± 24
403	Kr87	0.210 ± 8%	1.08	4.89	398 ± 32
845	-	0.043 ± 19%	1.06	2.44	165 ± 31
2555	-	0.015 ± 16%	1.05	0.87	167 ± 27
196	Kr88	0.198 ± 15%	1.12	9.56	185 ± 28
362	-	0.021 ± 58%	1.09	5.39	35 ± 21
835	-	0.060 ± 15%	1.06	2.47	228 ± 34
1530	-	0.038 ± 15%	1.05	1.40	255 ± 38
2196	-	0.031 ± 14%	1.05	1.00	291 ± 41
2392	-	0.059 ± 8%	1.05	0.92	607 ± 49
898	Rb88	0.048 ± 20%	1.06	2.30	196 ± 39
1836	-	0.034 ± 13%	1.05	1.18	276 ± 36
81	Xe133	0.215 ± 22%	1.19	9.3	194 ± 43
250	Xe135	1.069 ± 3%	1.10	7.64	1272 ± 38
527	Xe135m	0.278 ± 5%	1.07	3.80	684 ± 34
258	Xe138	0.338 ± 6%	1.10	7.42	414 ± 25
396	-	0.037 ± 34%	1.08	4.97	69 ± 24
435	-	0.111 ± 13%	1.08	4.55	226 ± 29
1768	-	0.033 ± 19%	1.05	1.22	257 ± 49
409	Cs138	0.029 ± 34%	1.08	4.82	55 ± 19
463	-	0.120 ± 11%	1.08	4.29	259 ± 28
548	-	0.026 ± 41%	1.07	3.66	65 ± 27
1010	-	0.043 ± 20%	1.06	2.07	195 ± 39
1436	-	0.093 ± 9%	1.06	1.49	591 ± 53
2218	-	0.019 ± 19%	1.05	0.99	182 ± 35

uncertainties (1 sd) from counting statistics only

4. MODEL CALCULATIONS

Both computer programs UNIDOSE and PLUCON use a stationary Gaussian plume model for atmospheric dispersion and a finite plume model for the calculation of the external gamma dose from the plume. The models have been compared with each other and with models from other Nordic countries (Thykier-Nielsen et al., 1978, and Thykier-Nielsen, 1979). The agreement was generally good.

The main difference between the two models is the determination of dispersion parameters. UNIDOSE calculates the dispersion parameters from an empirical formula, based on smoke-puff measurements at Studsvik. The formula is given by Högström (1964, 1968). PLUCON uses normally the dispersion parameters given by Turner (1969) for 6 stability classes A-F according to the Pasquill-stability classification. Furthermore, the models differ somewhat with respect to numerical methods.

Both models use gamma-ray buildup factors based upon Monte Carlo calculations of infinite air media and source depletion for the calculation of dry deposition.

4.1. Description of UNIDOSE

UNIDOSE is a program system designed for calculation of consequences from a radioactive release to the atmosphere. The external gamma dose from the plume and from the ground and the internal dose from inhalation is calculated. Dry and wet deposition, radioactive decay as well as growth and decay of daughter products is considered in the program. Figure 13 outlines the basic elements of the program.

Only those formulas with special interest in this study will be given here, a full description is given by Karlberg (1979).

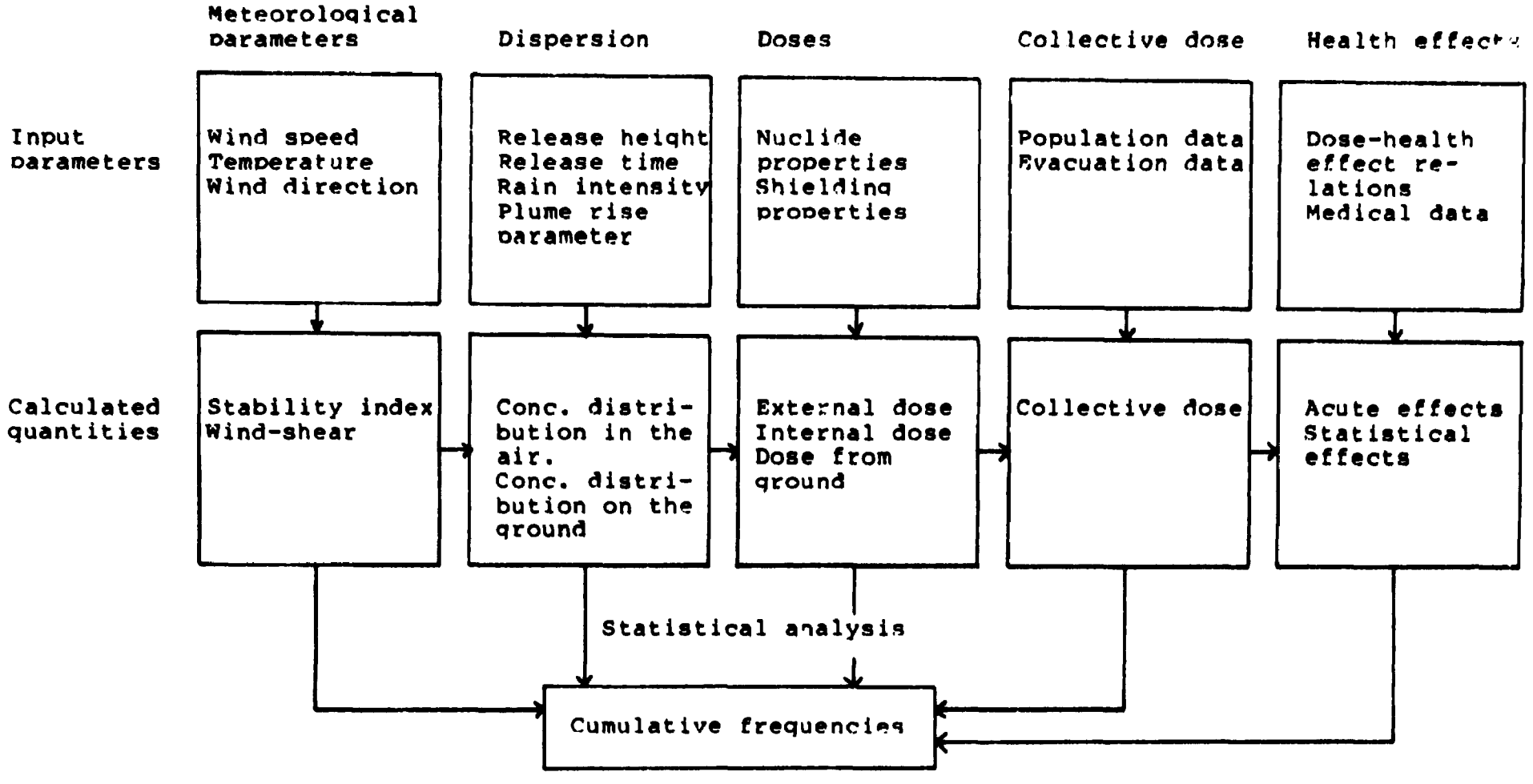

Fig.13. Basic elements of UNIDOSE.

The activity concentration relative to a coordinate system with origin at the source point at the effective release height, the x-axis in the wind direction and vertical z-axis is given by:

$$\chi(x,y,z) = \frac{Q}{2\pi\,\sigma_y(x)\,\sigma_z(x)\,u} \exp\left(-\frac{1}{2}\frac{y^2}{\sigma_y(x)^2}\right) \cdot \left\{\exp\left(-\frac{1}{2}\frac{z^2}{\sigma_z(x)^2}\right) + \exp\left(-\frac{1}{2}\frac{(z+2h)^2}{\sigma_z(x)^2}\right)\right\}$$

where

$\chi(x,y,z)$ = activity concentration

Q = release rate of activity

u = wind speed at release height

$\sigma_y(x)$, $\sigma_z(x)$ = dispersion parameters

h = effective release height

The activity concentration at ground level is given by:

$$\chi(x,y,-h) = \frac{2Q}{2\pi\,\sigma_y(x)\,\sigma_z(x)\,u} \exp\left\{-\frac{1}{2}\left(\frac{y^2}{\sigma_y(x)^2} + \frac{h^2}{\sigma_z(x)^2}\right)\right\}$$

In UNIDOSE, the dispersion parameters are calculated using an empirical formula given by Högström (1964, 1968). The dispersion parameters are assumed to be continous functions of the stability index, s, given by:

$$s = \frac{(dT/dz + 1) \cdot 1000}{u_f^2}$$

where

dT/dz = temperature gradient ($^{o}C/100$ m)

u_f = the geostrophical wind speed (m/s)

The relationship between the dispersion parameters and the stability index, s, was found in smoke-puff measurements. The formulas are quite complex and will not be given in detail here. The variation with distance x is however:

$$\sigma_y = K_y \sqrt{\exp(-A_y x) + A_y x - 1}$$

$$\sigma_z = K_z \sqrt{\exp(-A_z x) + A_z x - 1}$$

where K_y is a function of s, and A_y is a constant depending on the topography. K_z is a function of s for winter months and a function of wind speed and release height for summer months. A_z is a function of wind speed and release height.

For unstable conditions, K_y has a topography-dependent value, and K_z is based on the wind speed, release height and time of year.

When σ_z exceeds the value of the mixing height, a uniform distribution in the vertical direction is assumed. The value of the mixing height could be given as input data or read from a meteorological file.

The dry deposition to the ground of radioactivity in the cloud is calculated with a standard scurce depletion model. The flux of activity deposited on the ground is given as a product of the deposition velocity, v_d, and the activity concentration at the ground level $\chi(x,y,-h)$.

<u>External gamma dose from the plume.</u> Assuming that the gamma-ray energies from the radionuclides in the plume are divided into energy groups, the ground level gamma dose in air from the cloud will be:

$$D(x,y) = K \sum_i^{n_e} E_i \mu_{en_i} \sum_j^{n_{is}} f_{i,j} \int_V \frac{B(\mu_i r) \exp(-\mu_i r)}{4\pi r^2} \chi_j(x,y,z)\,dV$$

where

K = conversion factor

n_e = number of energy groups

E_i = mean energy of group i

μ_i^{en} = energy absorbtion coefficient for air in group i

n_{is} = number of nuclides

$f_{i,j}$ = photon yield for nuclide j in group i

μ_i = attenuation coefficient for air in group i

r = distance between detector position and volume element dV

$B(\mu_i\ r)$ = build-up factor for energy group i

$\chi_j(x,y,z)$ = concentration distribution of nuclide j

This integral is solved in a straightforward manner with numerical integration in all three directions. Due to the singularity, low-order numerical methods are used, i.e. the trapezoidal method in y and z direction and Simpsons method in the x direction.

A small volume around the singular point is excluded from the numerical integration and solved analytically with constant values of all variables except the $1/r^2$ factor.

The primary photon flux from nuclide j in energy group i is calculated in a similar way

$$\Phi(x,y) = f_{i,j} \int_V \frac{\exp(-\mu_i\ r)}{4\pi r^2}\ \chi_j\ dV$$

The calculation of the external gamma dose and the primary photon flux at 1 metre above the surface from radionuclides on the ground is done in a similar way with a two-dimensional integration over an infinite disk source. Only a relatively small area contributes to the total dose, and the source concentration is therefore assumed constant over the whole disk and equal to the value under the point of interest.

The integrated dose over a time interval is calculated with consideration taken to the build-up and decay of the surface

activity. The start and end of deposition and exposure can be assigned arbitrarily.

The growth and decay of daughter products are considered in the calculation of air concentration, external gammma dose from the cloud and from the ground. Consideration is also taken to whether the parent nuclide or the daughter or both are reactive and thus contributes to the deposition on the ground.

4.1.1. Simulations of the experiments with UNIDOSE

The following quantities were used in the model calculations:

Quantity	Comparision based on measurement with
Relative concentration	SF_6-tracer sampling equiment
Total gamma-ray exposure	Ionisation chambers and GM-detectors
Primary gamma-ray fluence	Germanium detectors

Three sets of parameters were used in the calculations:

1. Standard parameters. Stability estimated from the 100-m meteorological mast at the power plant.

2. Standard parameters. Stability estimated from the 11-m mast at Värö backa.

3. Best estimated parameters. Dispersion parameters estimated from the SF_6 measurements. The primary gamma-ray fluence was calculated with these parameters only.

The parameter values used in the calculations are listed in Table 17. The best estimates given for dry deposition are explained

in section 4.3. The best estimates of the dispersion parameters are based upon a horizontal dispersion parameter (σ_y) derived from the observed crosswind concentration distribution (SF_6), and a vertical dispersion parameter (σ_z) inferred from mass balance considerations. In experiments I and IV, however, it was not possible to determine the vertical dispersion parameter from mass balance calculations. The observed concentrations were higher than could be accounted for by the model. Therefore, the effective release heights were taken as the vertical dispersion parameters in these two cases, as this maximises the calculated concentrations.

Table 17. Parameter values used in UNIDOSE calculations

	Experiment			
Parameter	I	II	III	IV
Release height (m)	139	199	147	119
Dry deposition (m/s)				
Standard		$3 \cdot 10^{-3}$		
Best estimate	$2 \cdot 10^{-2}$	-	$10 \cdot 10^{-2}$	$10 \cdot 10^{-2}$
Wind speed (m/s)	8.5	3.5	8.0	13.5
Stability index s				
From 100-m mast	neg.	10.6	neg.	neg.
From 11-m mast	0	-	0	0
(neg.= unstable, 0 = neutral)				
Downwind distance (km)	4.1	2.9	3.1	3.1

Table 18 shows some intermediate results from the calculations.

The calculated crosswind distributions of relative concentrations and of the total gamma-ray exposures (cloud- and groundshine) are shown in Fig. 14 together with the measured data. Each calculated profile has been given the same center of mass as that from the SF_6-measurement.

Table 18. Calculated and measured dispersion parameters.

	Experiment			
Quantity	I	II	III	IV
σ_y (m)				
1. Calc. (100-m mast)	327	157	243	243
2. - (11-m mast)	243	-	179	179
3. Est. from SF_6	299	-	195	160
σ_z (m)				
1. Calc. (100-m mast)	235	107	223	193
2. - (11-m mast)	146	-	132	114
3. Est. from SF_6	139	-	69	119

Tables 19 - 21 show the ratios between measured and calculated primary gamma-ray fluences for the three spectrometer measurements. The dispersion parameters estimated from the SF_6-measurements were used for these calculations. Only the detected radiations from each nuclide are included in the calculation of the gamma-ray fluence for each energy group. In order to facilitate a comparison between UNIDOSE and PLUCON, UNIDOSE has used the same energy groups as PLUCON (see Section 4.2).

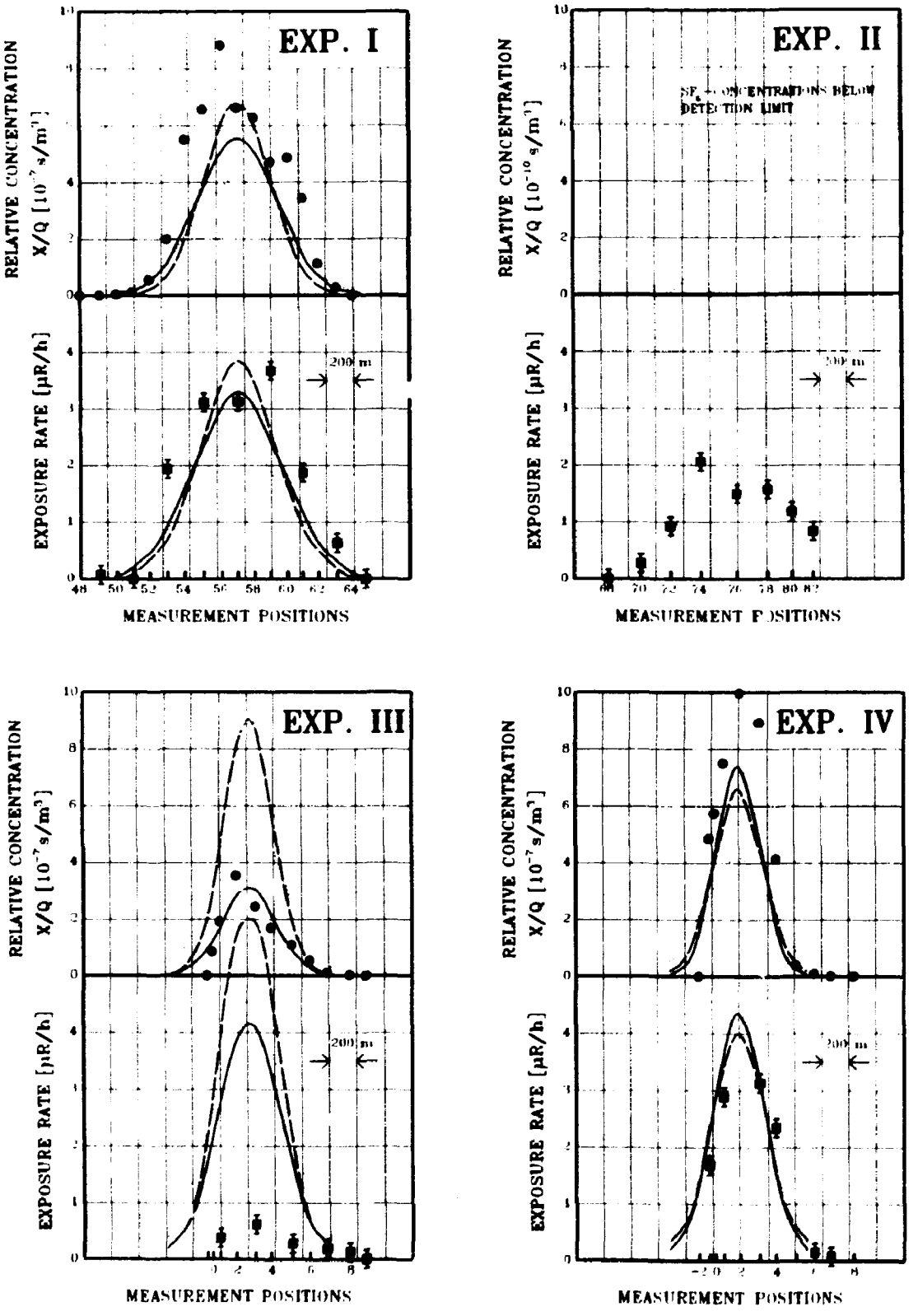

Fig.14. Crosswind distributions calculated with UNIDOSE of relative concentrations and gamma-ray exposures. The measured values are shown for comparison. Dispersion parameters estimated from 1).....100-m mast measurements, 2)_ _ _ 11-m mast measurements and 3)_____ SF_6-measurements.

Table 19. Relative primary gamma-fluence rates (measured/calculated) in experiment I at position 55. For the noble gas daughters the calculations include a contribution from ground deposition (v_d=0.02 m/s).

	Energy group							
Nuclide	2	3	4	5	6	7	8	mean
Kr85m		0.97 ± 0.04	0.78 ± 0.21					0.88
Kr87			0.86 ± 0.05	0.80 ± 0.20		1.35 ± 0.27	0.70 ± 0.10	0.93
Kr88		1.22 ± 0.15	1.24 ± 0.19			0.73 ± 0.07	1.04 ± 0.04	1.06
Xe133	1.22 ± 0.13							1.22
Xe135m				0.97 ± 0.04				0.97
Xe135		1.32 ± 0.02		0.64 ± 0.75				0.98
Xe138		1.93 ± 0.42	1.06 ± 0.07			1.25 ± 0.08	0.69 ± 0.43	1.23
mean	1.22 ± 0.13	1.25 ± 0.02	0.94 ± 0.04	0.96 ± 0.04		0.97 ± 0.05	0.99 ± 0.04	1.04
Rb88					1.74 ± 0.21	1.78 ± 0.12		1.76
Cs138			1.70 ± 0.17	1.82 ± 0.22	1.23 ± 0.12	1.33 ± 0.07	1.20 ± 0.23	1.46
mean			1.70 ± 0.17	1.82 ± 0.22	1.36 ± 0.10	1.44 ± 0.06	1.20 ± 0.23	1.61

Table 20. Relative primary gamma-fluence rates (measured/calculated) in experiment I at position 59. For the noble gas daughters the calculations include a contribution from ground deposition (v_d=0.02 m/s).

	Energy group						
Nuclide	2	3	4	5	6	7	8	mean
Kr85m		0.84 ± 0.18						0.84
Kr87			1.06 ± 0.09					1.06
Kr88		1.26 ± 0.17						1.26
Xe135		1.32 ± 0.07						1.32
Xe135m				1.10 ± 0.11				1.10
Xe138			1.10 ± 0.17			1.19 ± 0.28		1.15
mean		1.26 ± 0.06	1.07 ± 0.08	1.10 ± 11		1.19 ± 0.28		1.12
Cs138			0.65 ± 0.08		0.44 ± 0.09	0.37 ± 0.04		0.49

Table 21. Relative primary gamma-fluence rates (measured/calculated) in experiment IV at position 4. For te noble gas daughters the calculations include a contribution from ground deposition (v_d=0.10 m/s).

	Energy group							
Nuclide	2	3	4	5	6	7	8	mean
Kr85m		1.35 ± 0.22	2.26 ± 0.76					1.99
Kr87			1.94 ± 0.15	4.46 ± 0.85			2.0 ± 0.32	2.80
Kr88		1.74 ± 0.26	4.45 ± 2.20	2.73 ± 0.41		2.45 ± 0.37	1.97 ± 0.12	3.10
Xe133	2.02 ± 0.45							2.02
Xe135		2.40 ± 0.07						2.40
Xe135m				1.76 ± 0.09				1.76
Xe137			3.29 ± 0.82					3.29
Xe138			2.44 ± 0.15			1.65 ± 0.31	3.20 ± 1.04	2.43
mean	2.02 ± 0.45	2.27 ± 0.06	2.21 ± 0.10	1.83 ± 0.09		1.98 ± 0.24	1.99 ± 0.11	2.47
Rb88					2.48 ± 0.50	2.12 ± 0.28		2.30
Cs138			1.91 ± 0.21	1.17 ± 0.48	1.17 ± 0.23	1.46 ± 0.15	1.80 ± 0.38	1.52
mean			1.91 ± 0.21	1.17 ± 0.48	1.40 ± 0.21	1.61 ± 0.13	1.80 ± 0.38	1.91

4.1.2. Uncertainty analysis

When comparing model calculations to measurements in the way it has been done in this report, a discrepancy could originate from mainly two reasons. One is the inadequacy of the model itself to describe the real events (in this case the Gaussian assumptions, etc.) and the uncertainty of the parametrisation (i.e. the method to determine the dispersion parameters from meteorological measurements).

The other is the uncertainty of the measured quantities (concentrations, exposure rates) and the uncertainties in the model response due to uncertainties in the measured input data (windspeed, release height etc.).

The conclusions from the comparison with the measured quantities are improved if an estimate of this latter type of uncertainty is available.

This could be done with an ordinary analytical method, but when the model becomes complex numerical methods are more practical. A computer program by Gardner et al.(1985), based on random (Latin hypercube) sampling technique, has been developed in order to determine the effects of parameter uncertainties. An uncertainty distribution (normal, log-normal, uniform etc.) is assigned to each selected parameter in the model. A large number of random samples are taken from these distributions and the model response for each set of samples is calculated. The distribution of the response is then calculated and with use of regression analysis, it is possible to calculate the contribution of each parameter to the total uncertainty of the model response.

The method was applied to experiment I with dispersion parameter set 1 (Table 18). The following distributions were assigned to the parameters:

Parameter	Distribution	Mean	St.dev.
Plume rise	Normal	29 m	40%
Wind speed	"	8.47 m/s	10%
Temp.gradient	"	- 2.2°c/100m	10%
Downwind distance	"	4100 m	100 m

The calculations gave the following results for the relative crosswind-integrated concentration:

Mean	$3.3 \cdot 10^{-4}$ s/m^2
St.dev	$3.6 \cdot 10^{-5}$ "
Measured value	$6.3 \cdot 10^{-4}$ "

The assumed parameter uncertainty thus caused an uncertainty of the mean of the relative crosswind-integrated concentration of 11%. The regression analyses show that this uncertainty is due mainly to to uncertainty in the wind speed (90%) and the uncertainty of the plume rise (7%). The assumed uncertainty of the plume rise has here only a minor influence of the overall uncertainty in the model response, mainly due to the high value of σ_z (235 m). For parameter set no. 2 (Table 18) and the same assumed uncertainties, the mean of the crosswind-integrated concentration was $4.1 \cdot 10^{-4}$ s/m^2 with a standard deviation of 13%. The contributions from wind speed and plume rise uncertainties are now 60% and 36%, respectively.

This simple analysis shows that only a minor part of the discrepancy between the calculated and the measured crosswind-integrated concentrations can be explained by parameter and measurement uncertainties. The main part must be explained by model inadequacy.

4.2. Description of PLUCON

PLUCON is a program designed for calculation of the consequences of a release of radioactive material to the atmosphere. The external gamma doses from the plume and from the material deposited on the ground are calculated as well as the internal doses from inhalation. Dry and wet deposition, radioactive decay as well as growth and decay of daughter products are accounted for in the program. Only those parts of the model which are relevant to this study will be described here. A detailed description is given elsewhere (Thykier-Nielsen, 1980).

According to the Gaussian dispersion model, the material is assumed to have a normal (Gaussian) distribution in the plane perpendicular to the wind direction. If it is further assumed that the surface of the earth is totally reflecting, then the dispersion formula in a rectangular coordinate system with x = 0 at the source point, z = 0 at the effective plume height, and the x-axis in the wind direction will be:

$$\chi(x,y,z,s,u) = Q(x,t)\ Sg(x,y,z,s,u)$$

as

$$Sg(x,y,z,s,u) = \frac{1}{2\ \pi\ u\ \sigma_y(x,s)\ \sigma_z(x,s)}$$

$$\exp\left(-\frac{y^2}{2\ \sigma_y(x,s)^2}\right)\ \left[\exp\left(-\frac{z^2}{2\ \sigma_z(x,s)^2}\right) + \exp\left(-\frac{(z+2\ H)^2}{2\ \sigma_z(x,s)^2}\right)\right]$$

where

$\chi(x,y,z,s,u)$	= concentration at a point with the coordinates (x,y,z)
$Sg(x,y,z,s,u)$	= relative concentration
(x,y,z)	= coordinates of the detector point
s	= category of atmospheric stability
u	= wind speed

$\sigma_y(x,s)$ = horizontal dispersion parameter
$\sigma_z(x,s)$ = vertical dispersion parameter
$Q(x,t)$ = apparent source strength at the time t
H = effective stack height

The concentration at ground level (z = -H) is calculated from

$$\chi(x,y,-H,s,u) = \frac{1}{\pi u \sigma_y(x,s)\ \sigma_z(x,s)} \exp\left\{-\frac{1}{2}\left(\frac{y^2}{\sigma_y(x,s)^2} + \frac{H^2}{\sigma_z(x,s)^2}\right)\right\}$$

If the dispersion conditions are markedly affected by a mixing layer which gives ar upward limit to the atmospheric layer in which the released material are dispersed then the formulas given above are modified according to a procedure given by Turner (1969).

In PLUCON, Turner's ten-minute average values for the dispersion parameters, $\sigma_y(x,s)$ and $\sigma_z(x,s)$, are used (Turner, 1969). The stability of the atmosphere is classified in 6 categories A-F (Pasquill, 1961).

These dispersion parameters can be used for release durations of up to half an hour. For longer release periods, $\sigma_y(x,s)$ is corrected according to a formula given in WASH 1400 (1975):

$$\sigma_y'(x,s) = \sigma_y(x,s)\left(\frac{t}{1800}\right)^{\frac{1}{3}}$$

where

$\sigma_y'(x,s)$ = corrected horizontal dispersion parameters
$\sigma_y(x,s)$ = horizontal dispersion parameter, 10-minute average
t = duration of release (s)

The dry deposition of material is calculated using the source depletion model.

The amount of material deposited on the ground per unit time per unit of area is:

$$W_D(x,y,s,u) = v_d \cdot \chi'(x,y,-H,s,u)$$

where

v_d = deposition velocity

$$\chi'(x,y,-H,s,u) = Q_D(x,t,s)\ S_g(x,y,-H,s,u)$$

= concentration of material above the ground corrected for deposition.

$Q_D(x,t,s)$ = source term corrected for deposition

$$= Q_o\ g_i(x,t)\ \exp\left(-\int_o^x \frac{v_d}{u \cdot \pi \cdot \sigma_z(x,s)} \exp\left(-\frac{1}{2}\left(\frac{H}{\sigma_z}\right)^2\right) dx\right)$$

where $g_i(x,t)$ is the decay function for isotope i.

External gamma doses from the plume

The external gamma radiation dose at a given point P (x_d, y_d, z_d) is found by integrating the radiation from the plume. If the plume contains n_{iso} isotopes whose photon energies are distributed on n_e energy groups, the gamma dose (in i.e. Sv) at point P is found to be:

$$D_G(x_d,y_d,z_d,s,u) = K \cdot \sum_{i=1}^{n_e} E_i^{\gamma}\ \sigma_i^{\gamma} \sum_{j=1}^{niso} f_{i,j} \int_V \frac{B(\mu_i r)\ \exp(-\mu_i r)}{4\pi r^2}\ \chi_j(x,y,z,s,u)\,dV$$

where

r^2 = $(x-x_d)^2+(y-y_d)^2+(z-z_d)^2$

s = stability category

K = conversion factor

n_e = number of energy groups

E_i^γ = mean photon energy in the i'th energy group

$\sigma_i^\gamma = \sigma(E_i^\gamma)$ = mass energy absorption coefficient for air, in the i'th energy group

$f_{i,j}$ = photon yield for isotope j, in i'th energy group

$\mu_i = \mu(E_i)$ = linear attenuation coefficient for air, in the i'th energy group

$B(\mu_i\ r)$ = buildup factor for the i'th energy group

η = shielding factor for buildings, etc.

n_{iso} = number of isotopes

A total of 8 energy groups are used with mean energies of 0.04, 0.12, 0.20, 0.38, 0.68, 1.09, 1.68 and 2.53 MeV.

The integration over three dimensions is carried out by means of Gauss-Christoffel quadrature with weight points calculated according to a method described by Gautchi (1981).

The primary photon flux from nuclide j in energy group i is calculated from

$$\Phi_{i,j}(x,y,z,s,u)=f_{i,j}\int_V \frac{\exp(-\mu_i\ r)}{4\pi\cdot r^2}\cdot \chi_j(x,y,z,s,u)dV$$

External gamma doses from deposited radioactive material

The external gamma dose from radioactive material deposited on the ground at a given point P is found by integrating the dose contributions from the ground. It is assumed in the calculation that the ground can be considered as an infinite, plane source, where the radioactive material is deposited with a uniform concentration, corresponding to the concentration on the ground directly under point P. The dose is calculated at 1 m above the ground.

$$D_S(x,y,s,u) = n\ \eta_g\ T \sum_{i=1}^{n_e} E_i^{\gamma}\ \mu_{en}(E_i)\ I_i^{*}(\mu_i\ 1)$$

$$\sum_{j=1}^{n_{iso}} f_{i,j} \int_{te_1}^{te_2} we_j(t,td_1) W_j(x,y,s,u,t,td_1,td_2)\,dt$$

where

$D_S(s,y,s,u)$ = external gamma dose 1 m above the ground from radioactive material deposited on the ground

$\mu_{en}(E_i^{\gamma})$ = linear energy absorption coefficient for air for photon energy E_i^{γ}

$\mu(E_i^{\gamma})$ = linear attenuation coefficient for air for the photon energy E_i^{γ}

i = energy group number ($1 \leq i \leq 8$)

j = isotope number

n_{iso} = number of isotopes

n_e = number of energy groups

E_i^{γ} = mean photon energy for energy group no. i

$f_{i,j}$ = photon yield for isotope j in the i'th energy group

$$I_i^*(\tau) = \int_{\tau}^{\infty} \frac{B_i(\rho)\, e^{-\rho}}{\rho} d\rho$$

$B_i(\rho)$ = buildup factor for the i'th energy group

$W_j(x,y,s,u,t,td_1,td_2)$ = concentration of isotope j on the ground vertically beneath the detector point at time t, when the deposition takes place from td_1 to td_2

$we_j(t,td_1)$ = correction factor for weathering of isotope j, at time t, when deposition starts at time td_1

te_1 = start of exposure

te_2 = end of exposure ended

td_1 = start of deposition started

td_2 = end of deposition

η = shielding factor for buildings, etc.

η_g = shielding factor for surface roughness

τ = correction factor for backscatter.

The primary photon flux is calculated in analogy to the photon flux from airborne radioactivity.

Buildup and decay of the isotopes and their daughter products are accounted for in the calculations. The depositability of a mother product and its daughter product do not have to be the same i.e. a mother product can be depositable and the daughter product not depositable, etc.

The gamma-ray buildup factor

The buildup factor used in calculation of gamma-ray doses is the one given by Capo (1958):

$$B(\mu(E)R) = \sum_{k=0}^{4} \beta_k(E) \quad (\mu(E)R)^k$$

where

$B(\mu(E)R)$ = buildup factor
E = photon energy
$\mu(E)$ = linear attenuation coefficient
R = distance from source to detector
$\beta_i(E)$ = polynomial coefficient

The formula applies when

$0 \leq \mu(E)R \leq 20$ when 0.255 MeV $\leq E \leq 10$ MeV

or

$0 \leq \mu(E)R \leq 7$ when $0.04 \leq E \leq 0.20$ MeV

The β-coefficients are given in Table 22.

The coefficients used for gamma-ray energies less than 0.2 MeV is based on Vrubel (1973). A discussion on the choice of buildup coefficients is given by Hedemann et al. (1980).

The gamma-doses are not very sensitive to the type of dose-buildup factor used. However, Capo's polynomial buildup factor has been chosen because it gives a good approximation to the experimental dose buildup data.

Table 22. β-coefficients for dose-buildup factor for air.

Energy group	Average energy [MeV]	β_0	β_1	β_2	β_3	β_4
1	0.04	9.999769E-1	2.189205E+0	1.631374E-1	5.579629E-3	2.090830E-4
2	0.12	1.057473E+0	2.098229E+0	1.161661E+0	-6.951280E-2	3.133146E-2
3	0.20	1.040584E+0	1.655762E+0	8.583238E-1	-4.527632E-2	2.244595E-2
4	0.38	9.919000E-1	1.125000E+0	7.032000E-1	3.107000E-2	0
5	0.68	1.001000E+0	9.454000E-1	3.444000E-1	2.183000E-3	0
6	1.09	9.960000E+0	9.838000E-1	1.449000E-1	-1.124000E-3	0
7	1.68	9.949000E-1	8.950000E-1	5.800000E-2	-9.131000E-4	0
8	2.53	9.967000E-1	7.470000E-1	2.032000E-2	-1.292000E-4	0

4.2.1. Simulations of the experiments with PLUCON

Calculations were made of the same quantities as in the previous section: relative concentrations, total gamma-ray exposures, and primary gamma-ray fluences.

Two sets of dispersion parameters were used. One was based on the standard Pasquill classification to determine the appropriate thermal stability class for which the Turner dispersion parameters was used. The other set contained the best estimates mentioned previously.

In experiment II the concentrations were below the detection limit, indicating no contact between the plume and the ground. Therefore, only the standard parameters were used in this case. Table 23 summarises the parameter values used for the calculations.

The resulting crosswind profiles of relative concentrations and total gamma exposures are shown in Fig. 15 together with the measured data. The detection limit of SF_6 in experiment II corresponds to $\chi/Q=2\cdot10^{-9}$ s/m^3. Each calculated profile has been given the same center of mass as that from the SF_6-measurement.

The results of the calculations of unscattered gamma radiation are shown in Table 24-26. The tables show ratios between measured and calculated gamma-ray fluence rates at the various spectrometer positions. The calculated gamma-ray fluence rates comprise the observed gamma-ray energies only. The dispersion parameters estimated from the SF_6-measurements were used for these calculations.

Table 23. Parameter values used in PLUCON calculations.

Parameter	Experiment I	II	III	IV
release height (m)	139	199	147	119
wind speed (m/s)	8.5	3.5	8.0	13.6
stability class	D	E	D	D
dispersion parmeters (m)				
σ_y-standard	316	182	245	245
-best estimate	299	-	200	160
σ_z-standard	78	43	65	65
-best estimate	139	-	68	119
deposition velocity (m/s)				
-standard	0.01	0.01	0.01	0.01
-best estimate	0.02	-	0.10	0.10
inversion layer height (m)	400	-	600	900
downwind distance (m)	4100	2900	3100	3100

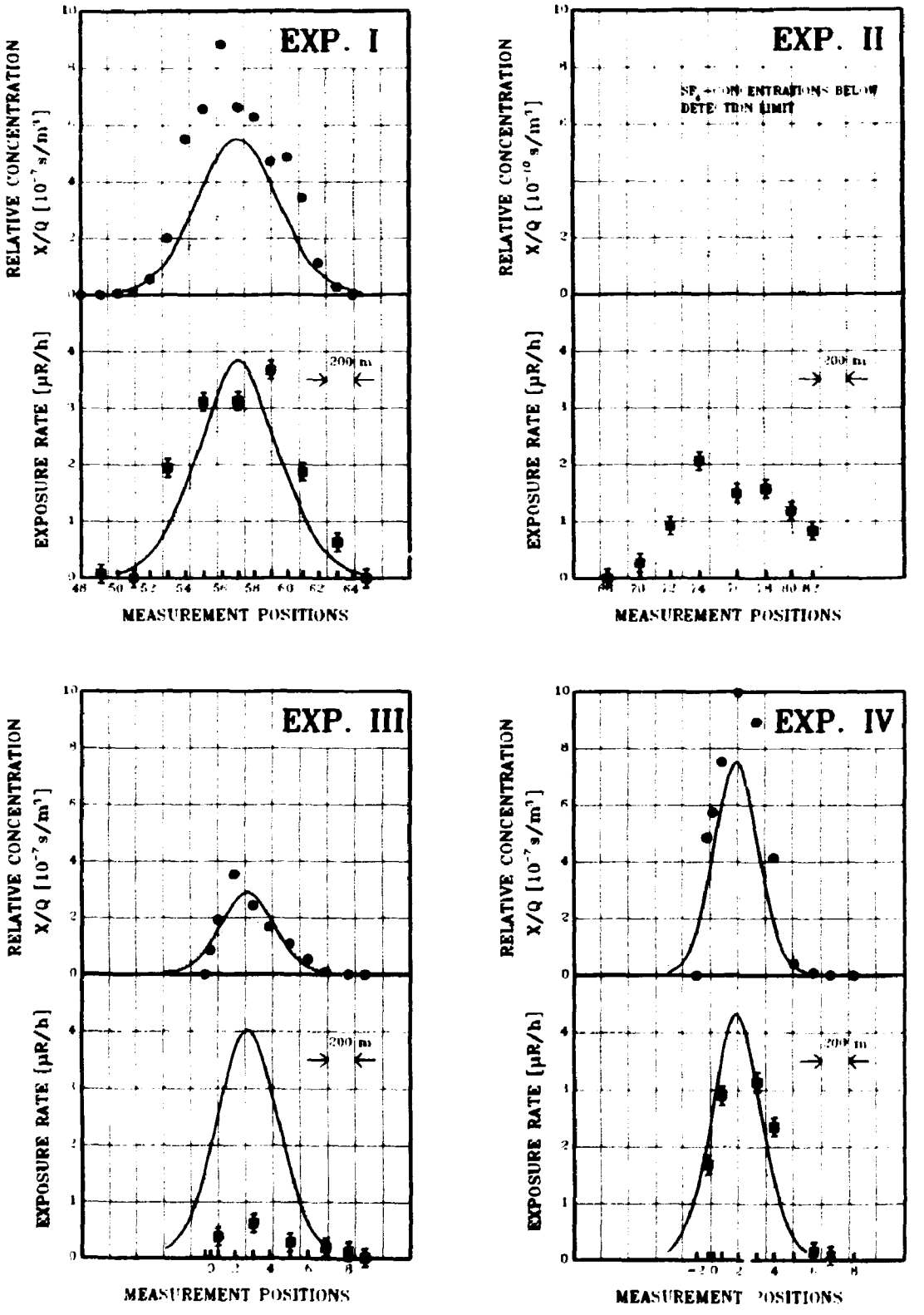

Fig.15. Crosswind distributions calculated with PLUCON of relative concentrations and gamma-ray exposures. The measured values are shown for comparison. Dispersion parameters estimated from 1)..... Pasquill stability classification based on 11-m mast measurements and 2)_____ SF_6-measurements.

Table 24. Relative primary gamma-fluence rates (measured/calculated) in experiment I at position 55. For the noble gas daughters the calculations include a contribution from ground deposition (V_d=0.02 m/s).

	Energy group							
Nuclide	2	3	4	5	6	7	8	mean
Kr85m		1.15±0.05	1.38±0.37					1.20±0.08
Kr87			1.60±0.08	1.66±0.33		1.71±0.33	1.16±0.13	1.50±0.13
Kr88		1.74±0.21		1.63±0.25		1.02±0.10	1.31±0.06	1.35±0.06
Xe133	1.74±0.19							1.74±0.19
Xe135		1.89±0.02						1.89±0.02
Xe135m				1.29±0.05				1.29±0.05
Xe138		1.25±0.27	1.48±0.06			1.63±0.11	0.89±0.55	1.52±0.07
mean	1.74±0.19	1.73±0.04	1.52±0.05	1.38±0.07		1.45±0.08	1.26±0.05	1.49±0.02
Rb88					1.29±0.15	1.35±0.09		1.32±0.08
Cs138			1.08±0.08	1.22±0.14	0.84±0.08	0.92±0.05	0.94±0.09	0.95±0.03
mean			1.08±0.08	1.22±0.14	0.98±0.07	1.01±0.04	0.94±0.09	1.02±0.03

uncertainties from counting statistics only

Table 25. Relative primary gamma-fluence rates (measured/calculated) in experiment I at position 59. For the noble gas daughters the calculations include a contribution from ground deposition. (V_d=0.02 m/s).

	Energy groups						
Nuclide	2	3	4	5	6	7	8	mean
Kr85m		1.29±0.24						1.29±0.24
Kr87			1.24±0.11					1.24±0.11
Kr88		1.71±0.24						1.71±0.24
Xe135		1.79±0.10						1.79±0.10
Xe135m				1.40±0.14				1.40±0.14
Xe138			1.48±0.17			1.06±0.26		1.35±0.14
mean		1.69±0.09	1.37±0.10	1.40±0.14		1.06±0.26		1.50±0.06
Cs138			1.15±0.14		0.82±0.16	0.69±0.08		0.80±0.07

uncertainties from counting statistics only

Table 26. Relative primary gamma-fluence (measured/calculated) in experiment IV at position 4. For the noble gas daughters the calculations include a contribution from ground deposition . (V_d=0.10 m/s).

	Energy groups							
Nuclide	2	3	4	5	6	7	8	mean
Kr85mr		1.96±0.33	3.67±1.05					2.29±0.34
Kr87r			2.71±0.22	5.84±1.10			2.60±0.42	3.05±0.22
Kr88r		2.54±0.38	4.25±2.55	3.64±0.54		3.18±0.47	2.05±0.16	2.75±0.22
Xe133	2.98±0.66							2.98±0.66
Xe135		3.48±0.10						3.48±0.10
Xe135m					2.37±0.12			2.37±0.12
Xe138			3.45±0.22			2.17±0.41		2.98±0.21
mean	2.98±0.66	3.08±0.11	3.20±0.17	2.83±0.15		2.58±0.31	2.56±0.15	2.88±0.07
Rb88					1.47±0.29	1.27±0.17		1.35±0.20
Cs138			1.06±0.12	0.68±0.28	0.69±0.14	0.77±0.07	1.13±0.22	0.84±0.05
mean			1.06±0.12	0.68±0.28	0.94±0.13	0.88±0.06	1.13±0.22	0.93±0.05

uncertainties from counting statistics only

4.3. Deposition of noble gas daughters

The radioactive material emitted from the reactor stack consists of noble gases only; particulates are retained in a filtration system. When the gases are released to the atmosphere their decay products of rubidium and caesium isotopes start to build up in the plume. These daughters deposit downwind on the ground and vegetation where the concentration reaches a maximum value which in case of stable conditions is determined by the rate of deposition and the rate of decay. Deposition is negligible for the noble gases (Sehmel, 1980). Therefore, gamma radiation from the gases needs to be considered only from the plume, whereas the gamma radiation from the daughters has two components: (1) the airborne part assumed to have a distribution similar to the gases and (2) the deposited part on the ground.

From an initial comparison between the gamma-spectrometric results and the model calculations it became evident that the measurements showed significant surplus of the gamma radiation from the daughters compared to that from the gases (these calculations were made without regard to deposition). This is illustrated in Fig. 16 showing ratios of measured-to-calculated fluence rates of unscattered gamma rays from the noble gases and their daughters. The fluence rates have been calculated with PLUCON using the best-estimated-sets of dispersion parameters and the ratios are given for the average energies of the energy groups used by PLUCON. The ratios for the gases deviate somewhat from unity, due to inadequacy of the model to describe reality. The obvious energy dependency of the daughter ratios is caused by not including deposition in the calculations.

Deposition velocities were estimated to account for the observed surplus of daughter radiation. The following simplifying assumptions were made. The situations were considered as stable with respect to release rates, wind direction, and other aspects related to atmospheric dispersion. Relevant time parameters in this context are the radioactive half-lives of ^{88}Rb and ^{138}Cs, which are 18 min and 32 min, respectively. Furthermore, the

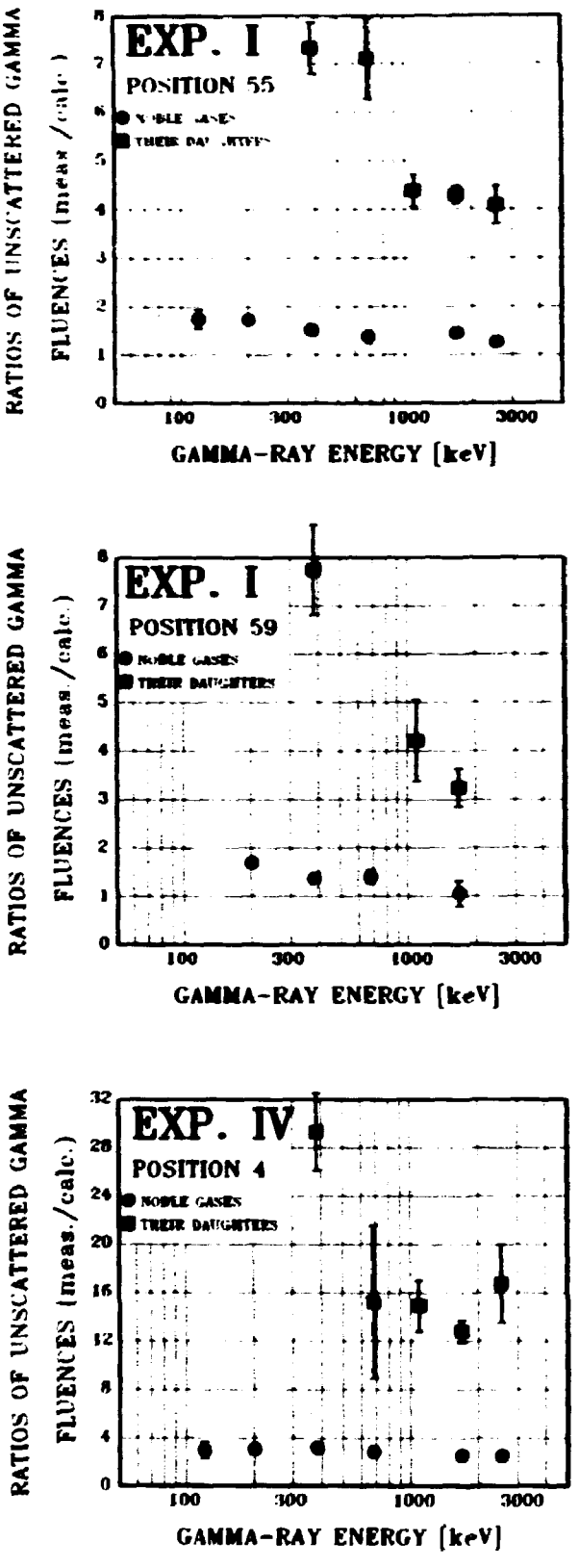

Fig.16. Ratios of measured-to-calculated unscattered gamma-ray fluence rates from the noble gases and their daughters at three measurement positions. The calculations were made with PLUCON without regard to deposition, and the ratios are given for the average gamma-ray energies of the energy groups used by the model.

distribution of the deposited daughters was considered to be that of an infinite plane source without regard to possible shielding from surface roughness and vegetation.

For each energy group in which daughter gamma radiation was detected, calculations were made with PLUCON to determine the deposition velocity which yields agreement between the measured and the calculated gamma-ray fluence rate. Care was taken not to include the undetected gamma rays from the daughters in these calculations. The results of the calculations are shown in Tables 27-29.

It is noted that there is good agreement between the two estimated deposition velocities of ^{138}Cs in experiment I at position 55 and 59. Furthermore, there seems to b tendency that the deposition velocities of ^{88}Rb are higher than those of ^{138}Cs. The average estimated deposition velocity in experiment I is 2 cm/s, and 10 cm/s in experiment IV. As the meteorological conditions in experiment III were rather similar to those in experiment IV, the deposition velocities in the two experiments were taken to be identical.

Table 27. Deposition velocities (cm/s) of noble gas daughters inferred from measurements and calculations at experiment I position 55.

	Energy groups					
Nuclide	4	5	6	7	8	mean
Rb88			2.5±0.4	2.7±0.3		2.6±0.2
Cs138	2.0±0.2	2.4±0.4	1.4±0.2	1.6±0.1	1.7±0.2	1.7±0.1
arithmetic mean						2.2

uncertainties from counting statistics only

Table 28. Deposition velocities (cm/s) of noble gas daughters inferred from measurements and calculations at experiment I position 59.

	Energy groups					
Nuclide	4	5	6	7	8	mean
Cs138	2.2±0.3		1.4±0.4	1.0±0.2		1.4±0.2

uncertainties from counting statistics only

Table 29. Deposition velocities (cm/s) of noble gas daughters inferred from measurements and calculations at experiment IV position 4.

	Energy groups					
Nuclide	4	5	6	7	8	mean
Rb88			13.6±3.2	11.2±1.8		11.8±1.6
Cs138	9.8±1.2	5.8±1.5	5.8±1.5	6.5±0.7	10.2±2.3	7.2±0.5
arithmetic mean						9.5

uncertainties from counting statistics only.

In the appendix the deposition velocities are calculated without regard to any dispersion model, nor to plume depletion, and based upon the same assumptions as above. This calculational procedure yields results quite similar to those obtained in this Section, showing that the estimated deposition velocities are independent of any particular dispersion model.

5. DISCUSSION

Meteorological measurements

The purpose of the meteorological measurement programme was to obtain information of the local wind field in order to carry out the experiments, and to document the meteorological conditions at the site during the experiments.

Two meteorological masts were available. One is the 100-m meteorological mast of the Ringhals nuclear power plant, positioned at the summit of a 15-m steep hill in a very inhomogeneous terrain. The measurements from this mast are suitable as guidance when carrying out experiments, but cannot form the basis for a detailed analysis of the meteorological conditions due to the inhomogeneous surroundings. Therefore, an 11-m meteorology mast was erected near Värobacka expecially for this campaign. The mast was instrumented in order to obtain the parameters needed for a detailed analysis of the local meteorology for the site. Such measurements ideally should be carried out over a completely homogeneous area, and we put much effort in finding a suitable position for the mast. During each experiment a radiosunde was launched near the small mast; it was mainly intended to give information about mixing heights.

Plume rise

The air that is released through the 110-m high ventilation stack has a vertical exit velocity of about 7 m/s and approximately a temperature of 31^{o}C. Due to the excess temperature the plume will tend to rise above the stack. However, wind blowing past the stack induces a wake on the lee side of it. If a plume is released with insufficient momentum and buoyancy it may be drawn into the wake and carried downward along the stack.

Very little guidance exists on the calculation of plume rise at such low excess temperatures, and the effect of downwash introduces an extra complication.

In the calculation of the final plume rise we have assumed that the individual plume rises that can be estimated for each of the various phenemena can be added together, and the result is the final plume rise. Consequently, the final plume rise was calculated by adding the plume rise due to buoyancy, the negative plume rise due to downdraft and a term that describes the effect on the plume rise due to the increased entrainment of air in a stack wake.

SF_6-tracer measurements

From Figs. 14 and 15 it is seen that the observed crosswind SF_6-tracer distributions comply well the model assumptions of Gaussian horizontal distributions. In Section 3.2.4, however, it is found that the measured concentrations in experiment I and IV are higher than can be accounted for by the model, which implies that in these cases the model assumptions of Gaussian vertical distributions cannot hold.

Experience with SF_6-tracer dispersion experiments (Gryning and Lyck, 1984) has shown that this problem is often encountered near the point of maximum ground-level concentration predicted by the Gaussian model. In experiments I, III, and IV the downwind distances to the tracer measurement line fall in this range.

Gamma-ray measurements

The precision of the radiation measurements has suffered from the very low levels of gamma radiation available during the experiments. The gamma-ray exposure rates from the plume and surface deposition ranged from 0 to about 4 μR/h and had to be determined in the presence of the natural background gamma radiation of about 6 μR/h. This yielded rather unfavourable signal-to-noise ratios.

Furthermore, the measurements of exposure rates with the GM-detectors were complicated by the varying gamma-ray-energy response of these detectors. It turned out that the gamma-ray energies from the noble gases and their daughters are so much

higher than those from natural background (including ^{137}Cs and ^{60}Co), that we had to apply an empirical correction factor for these detectors. This factor was derived from simultaneous measurements with GM-counters and ionisation chambers. The ionisation chambers have been shown by Beck (1982) to yield reliable exposure rates in the case of high-energy gamma radiation.

The measured exposure rates and unscattered gamma-ray fluences are consistent, which is seen from the exposure buildup factor combined for all gamma-ray energies. This factor is defined as the ratio of the exposure rate from all gamma rays to that from unscattered gamma rays alone. The unscattered gamma-ray fluence-rates are readily expressed in units of exposure rate by multiplication with the gamma-ray energies and the mass-absorption coefficients of air at these energies. A mean buildup factor of 1.7±0.1 was found at the two gamma-spectrometric observations (experiment I pos. 55 and experiment IV pos. 4), where the energy intervals included all the gamma-rays from the noble gases. The corresponding mean buildup factor was calculated from the PLUCON model at a value of 1.4±0.1, and this value is considered to be more correct. The experimental value is believed to be higher due to an underestimate of the unscattered gamma radiation, since many weak gamma lines from the noble gases and their daughters have remained undetected. This underestimate is inevitable and is caused by the inherent detection limit of the gamma-spectrometric measuring technique. For ionisation chambers and GM-detectors a similar underestimate is not manifest.

The relatively low buildup factor of 1.4 reflects the hard gamma radiation from the noble gases, which are dominant in the exposure rates. Both of the models UNIDOSE and PLUCON use buildup factors derived from Monte Carlo calculations of infinite air media and neglect the air-ground interface effect as discussed by Jacob et al. (1985), but this effect is small for hard gamma-rays.

Comparison of UNIDOSE and PLUCON

From Figs. 14 and 15 it is seen that the two models give identical results of concentrations and exposure rates for the same set of dispersion parameters (the so-called best estimates). The differences between the calculated profiles for the other parameters reflect the different ways used by the two models to calculate the dispersion parameters (the Högström system versus the Pasquill-Gifford-Turner system). From the calculations of unscattered gamma fluence rates, however, there seems to be some inconsistencies between the two models for which we have no current satisfactory explanations.

Deposition velocities

The estimated deposition velocities are very high considering the current view of this parameter in the context of radiological consequences of nuclear accidents (Gjørup et al., 1985). From the assumptions made, however, these estimates may be characterized as realistic, not as conservative. The deposition velocities would have been even higher if the assumptions of stable release rates, wind directions, and other aspects related to atmospheric dispersion were not true, and if shielding due to surface roughness and vegetation was not negligible.

Considering the circumstances the deposition velocities are not unrealistically high. In experiment I the wind speed at the 96-m height was 8 m/s and the roughness length at the measurement positions was about 3 cm (agricultural fields). This yields a maximum possible deposition velocity ($=u_*^2/u$, where u_* is the friction velocity and u the wind speed) of 3 cm/s (Thykier-Nielsen and Larsen, 1982), which does not contradict our estimate of 2 cm/s. In experiment IV the wind speed at the 96-m height was 14 m/s and the roughness length at the measurement positions was about 100 cm (mainly coniferous trees), which yields a maximum possible deposition velocity of about 20 cm/s. Again this is not inconsistent with our estimate of 10 cm/s.

The reason for these high deposition velocities is found in the combination of the wind speed, surface roughness and size of the daughter particles. As mentioned previously, the daughters start to build up in the air after release of the noble gases to the atmosphere. This leaves only the transport time (8 min in experiment I and 4 min in experiment IV) for the daughters to build up and to attach to airborne particles, and therefore the size of the noble gas daughter particles must be very small. The size distribution of the noble gas daughter particles present during the experiments may probably be approximated with that of free radon daughters, which have a mean particle diameter of about 1 nm (Porstendörfer, 1984). Predicted deposition velocities for such small particles are several orders of magnitude greater than the minimum deposition velocities which are found for particles with mean diameters in the range of 0.1 - 1 µm (Sehmel, 1980).

The estimated deposition velocities seem to indicate a higher rate of deposition (about 60%) of ^{88}Rb than that of ^{138}Cs. This trend is in agreement with the figures reported by Sehmel (1980).

The deposition of noble gas daughters on vegetation has been documented directly from measurements of grass samples collected downwind at the Ringhals power station (Aronsson, 1983).

Model calculations versus measurements.

The experiments reflect some of the advantages and some of the shortcomings of the Gaussian dispersion model. Among the advantages is the ability to calculate concentrations and doses with a rather simple mathematical model, and among the shortcomings are the meteorological assumptions which often do not apply well to reality. Furthermore, the experiments illustrate that even when the horizontal plume dispersion is well approximated with a Gaussian distribution, this may not be the case for the vertical distribution.

In experiments I and IV there is fair agreement between measurements and calculations of concentrations and exposure rates. In experiment III, however, the measured exposure rates are lower than the calculated values by a factor of about 5, while the measured concentrations are modelled very well. We have no satisfactory explanation for this, but we believe that it is connected to the vertical distribution of the plume.

One fundamental difference between the measurements of concentrations and that of radiation is that the air-samples are collected at individual locations whereas the radiation is detected from a huge volume of air (and ground) surrounding the detector. The observed concentrations yield no direct information on the structure of the vertical distribution in contrast to the observed exposure rates and unscattered gamma-ray fluence rates. As a matter of fact if the radiation levels had been high enough to make the uncertainties from counting statistics insignificant, it would have been possible to estimate the vertical dispersion parameter from the gamma-spectrometric measurements due to the different attenuations in air for gamma-rays of different energies.

The measured concentrations in experiment I and IV are somewhat higher than the models can account for. This is believed to be due to non-Gaussian vertical distributions. The measured exposure rates compare better with the calculated values. The reason for this is that these calculations were made with the estimated deposition velocities, and the noble gas daughters deposited on the ground contribute up to 35% of the exposure rate from the plume.

In experiment II which was made at midnight under atmospherically stable conditions the plume passed directly over the measurement positions. The stable conditions are of particular interest with regard to radiological consequences of nuclear accidents due to the relatively low dilution of the effluent. It is noted that the calculated exposure rates for both models are higher than the measured values.

Calculations were made of concentrations and exposure rates with standard parameters and with parameters estimated from the SF_6 measurements for both models (Fig. 14 and 15). These results illustrate that when detailed information on the dispersion parameters is available, the stationary Gaussian dispersion models can predict concentrations and doses quite well. In most cases, however, when the meteorological data make it necessary to use the standard dispersion parameters, the model predictions are less accurate.

Fig.17. The experimental team with the nuclear power station in the background (Gunner Dalsgaard, Hans Ahleson, Henrik Prip, Arent Hansen, Olof Karlberg, Sven Poul Nielsen, Eric Lyck, and Sven-Erik Gryning).

ACKNOWLEDGEMENTS

The authors wish to thank Carl Gunnar Mattsson and Per Olof Aronsson for valuable assistance at the Ringhals power plant during the experiments. We are grateful to Bernt Serby, Hans Ahleson, Bjarne Breiting, Arent Hansen, Gunner Dalsgaard, and Henrik Prip for conscientious work during the campaign often during late hours of the day.

The work was partly financed by the Nuclear Safety Board of the Swedish Utilities and by the Danish association of utilities in Jutland and on Funen, Elsam.

REFERENCES

ARONSSON, P.O. (1983). The Ringhals power plant. Private communication.

BECK, H.L., DECAMPO, J.A. and GOGOLAK, C.V. (1972). In Situ Ge(Li) and NaI(Tl) Gamma-Ray Spectrometry. HASL-258. 75p.

BECK, H.L. (1982). Spectral Composition of the γ-Ray Exposure Rate due to Noble Gases Released during a Reactor Accident. Health Phys. 43, 335-343.

BRIGGS, G.A. (1969). Plume Rise. TID-25075 (Oak Ridge National Laboratory, Tennessee) 81p.

BRIGGS, G.A. (1981). Plume Rise and Buoyancy Effects. In: Atmospheric Science and Power Production. Ed. by D. Randerson, DOE/TIC-27601. (Technical Information Center, Springfield, VA) p. 327-366.

BØTTER-JENSEN, L. (1982). Calibration and Standardization of Instruments for Background Radiation Monitoring. I: 3rd International Symposium on Radiological Protection. Advances in Theory and Practice. Proceedings, Inverness, 6-11 June 1982. Vol. 2. (Society for Radiological Protection, Reading) 685-690.

CAPO, M.A. (1958). Polynomial Approximation of Gamma-ray Buildup Factors for a Point Isotropic Source, (General Electric, Cincinnati, Ohio) PEX-510.52 p.

CSNI/NEA (1984). International Comparison Study on Reactor Consequence Modelling. (OECD/NEA, Paris) 110 p.

DECAMPO, J.A., BECK, H.L. and RAFT, P.D. (1972). High Pressure Argon Ionization Chamber Systems for the Measurement of Environmental Radiation Exposure Rates. (New York Operations Office, N.Y.) HASL-260. 68p.

DYER, A.J. (1974). A review of flux-profile relationships. Bound.-Layer Meteorol. 7, 363-372.

GARDNER, R., ROJDER, B. and BERGSTROM, U. (1985). PRISM, A systematic Method for Determining the Effect of Parameter Uncertainties on Model Predictions. STUDSVIK (to be published).

GAUTCHI, W. (1968). Construction of Gauss-Christoffel Quadrature Formulas, Mathematics of Computation. 22: 251-270.

GJØRUP, H.L., JENSEN, P.H., LAURIDSEN, B., ROED, J. and WARMING, L. (1985). Deposition, Retention, and Decontamination of Radioactive Material on Urban Surfaces - Danish Program. Proceedings of a workshop on methods for assessing the off-site radiological consequenses of nuclear accidents, held by DG V, Commission of the European Communities, Luxembourg 15-19 April 1985.

GOGOLAK, .V. (1984). Rapid Determination of Noble Gas Radionuclide Concentrations in Power Reactor Plumes. Health Phys. 4, 783-792.

GOLDER, D. (1972). Relations among stability parameters in the surface layer. Boundary-Layer Meteorol., 3, 47-58.

GRYNING, S.E., (1981). Elevated source SF_6-tracer dispersion experiments in the Copenhagen area. Risø-R-446. Risø National Laboratory. 187 pp.

GRYNING, S.E., and THOMSON, D.W. (1979). A tall-tower instrument system for mean and fluctuating velocity, fluctuating temperature and sensible heat flux measurements. J. Appl. Meteorol., 18, 1674-1678.

GRYNING, S.E., and LYCK, E. (1980). Medium-range dispersion experiments downwind from a shoreline in near neutral conditions. Atmos. Environ., 14, 923-931.

GRYNING, S.E., and LYCK, E. (1984). Atmospheric dispersion from elevated sources in an urban area: comparison between tracer experiments and model calculations. J. Clim Appl. Meteorol., 23, 651-660.

HANNA, S.R., BRIGGS, G.A., and HOSKER, R.P. (1982). Handbook on Atmospheric Diffusion. DOE/TIC 11223. (Technical Information Center. U.S. Department of Energy, Oak Ridge, Tenn.)

HEDEMANN-JENSEN, P., and THYKIER-NIELSEN, S. (1980). Recommendations on Dose Buildup Factors used in Models for Calculating Gamma Doses from a Plume. RISØ-M-2204. (Risø National Laboratory, Roskilde, Denmark) 50 p.

HÖGSTRÖM, U. (1964). An Experimental Study on Atmospheric Diffusion. Tellus 16, 205 - 251.

HÖGSTRÖM, U. (1968). A Statistical Approach to the Air Pollution Problem of Chimney Emission. Atmos. Environ. 2, 251-271.

JACOB, P., and PARETZKE, H.G. (1935). Air-Ground Interface Correction Factors for Gamma-Emitters in Air. Health Phys. 48, 183-191.

KARLBERG, O., SCHWARTZ, H., FORSSÉN, B.-H., and MARKLUND, J.E. (1979). UNIDOSE - A Computer Program for the Calculation of Individual and Collective Doses from Airborne Radioactive Pollutants. Studsvik - 79/1, (Studsvik Energiteknik AB, Sweden) 52 p.

KARLBERG, O., NIELSEN, S.P., and THYKIER-NIELSEN, S. (1980). Measurements and Calculations of Atmospheric Dispersion of Radioactive Noble Gases from a Nuclear Power Plant. [In:] Seminar on Radioactive releases and their dispersion in the atmosphere following a hypothetical reactor accident. Proceedings 22 - 25 April 1980, Risø, Roskilde, Denmark. (Commission of the European Communities, Luxembourg) p. 925-951.

PASQUILL, F. (1961). The estimation of the dispersion of windborne material, Meteor. Mag. 90,33-49.

PORSTENDORFER. J. (1984). Behaviour of Radon Daughter Products in Indoor Air. Radiat. Prot. Dosim. 7, 107-113.

SEHMEL, G.A. (1980). Particle and Gas Dry Deposition: A Review. Atmos. Environ. 14, 983-1011.

STROEM, L., and KARLBERG. O. (1980). Measurements of the Stack-flow at Ringhals 1. STUDSVIK K2-80/305 (In Swedish).

THYKIER-NIELSEN, S., SEPPO, V., TVETEN, U., GYLLANDER, C., KARLBERG, O., and THOMASSEN, D. (1978). Comparison of Nordic Dose Models. Risø-M-1972. (Risø National Laboratory, Roskilde, Denmark) 199 p.

THYKIER-NIELSEN, S. (1979). Comparison of Nordic Models for Calculation of External Gamma Doses from a Plume. (Risø National Laboratory, Roskilde, Denmark) 11 p.

THYKIER-NIELSEN, S. (1980). The Risø Model for Calculating the Consequences of the Release of Radioactive Material to the Atmosphere. Risø-M-2214. (Risø National Laboratory, Roskilde, Denmark) 65 p.

THYKIER-NIELSEN, S., and LARSEN, S.E. (1982). The Importance of Deposition for Individual and Collective Doses in Connection with Routine Releases from Nuclear Power Plants. Risø-M-2205. (Risø National Laboratory, Roskilde, Denmark) 55p.

TURNER, D.B. (1969). Workbook of Atmospheric Dispersion Estimates. Rev.ed. (National Air Pollution Control Association, Cincinatti, Ohio). (Public Health Service Publication No. 999-AP-26) 84p.

UNSCEAR (1982). United Nations Scientific Committee on the Effects of Atomic Radiation. Ionizing radiation: sources and biological effects: 1982 report to the General Assembly, with anexes. (United Nations, New York) 773p.

VRUBEL, M.N., SIDNENA, S.N., and STRELKOV, A.S. (1973). Buildup Factors for Gamma Radiation scattering from a Point Source in an Infinite Air Medium. Atomnaya Energiya 34, (In Russian). 47 - 49.

WASH 1400 (1975). Reactor safety study An Assessment of Accident Risks in U.S. Commercial Nuclear Power Plants, Appendix VI, (NUREG-75/014) (US Nuclear Regulatory Commission, Washington, D.C)

APPENDIX

Estimation of deposition velocities of noble gas daughters

From a few simplifying assumptions it is possible to estimate the deposition velocities of the noble gas daughters without the use of dispersion models.

The air concentrations of the noble gases and of the noble gas daughters at the measurement positions during the experiments can be derived from the SF_6-concentrations. The relative SF_6-concentrations are multiplied with the release rates of the noble gases from Table 9, and a factor f to account for either decay of the gases or ingrowth of the daughters. For the daughters the factor f is calculated according to

$$f = (\exp(-\lambda_m t)-\exp(-\lambda_d t)) \cdot \lambda_d/(\lambda_d-\lambda_m),$$

where λ_m and λ_d are the decay constants for the mother-product and the daughter-product, respectively, and t is the transport time. It is assumed that deposition removes only an insignificant amount of activity compared to the total daughter activity in the plume.

The transport time in experiment I was 8.1 min and in experiment IV 3.8 min. The relative concentrations from the SF_6-measurements are shown in Table A1. The radioactive half-lives used are shown in Table A2, and Table A3 lists the calculated concentrations C_1.

Table A1. Relative concentrations obtained from the SF_6-measurements.

Experiment	Position	χ/Q (s/m^3)
I	55	$6.62 \cdot 10^{-7}$
I	59	$4.76 \cdot 10^{-7}$
IV	4	$5.15 \cdot 10^{-7}$

Table A2. Radioactive half-lives

Isotope	T(1/2)
Kr 85 m	4.48 h
Kr 87	1.272 h
Kr 88	2.84 h
Rb 88	17.8 min
Xe 133	5.245 d
Xe 135	9.09 h
Xe 135 m	15.29 min
Xe 138	14.17 min
Cs 138	32.2 min

Table A3. Estimated radionuclide concentrations in the air, C_1 (Bq/m^3), based upon SF_6-measurements.

Isotope	Exp. I pos. 55	Exp. I pos. 59	Exp. IV pos. 4
Kr 85 m	17.6	12.7	10.1
Kr 87	34.0	24.5	17.9
Kr 88	40.1	28.8	22.3
Rb 88	11.0	7.9	3.1
Xe 133	25.3	18.2	16.6
Xe 135	58.5	42.1	32.2
Xe 135 m	25.7	18.5	16.6
Xe 138	36.5	26.3	21.2
Cs 138	7.1	5.1	1.84

From the gamma-spectrometric measurements the radionuclide concentrations in the air can be inferred from the assumption of the semi-infinite cloud model. According to this model the concentration C_2 is given by

$$C_2 = 2\mu\phi/y$$

where μ is the linear attenuation coefficient for air, ϕ is the unscattered gamma fluence density and y is the gamma yield.

The Tables A4, A5, and A6 show the concentrations C_1 and C_2 and the ratios C_2/C_1 for the three gamma-spectrometric observations. The ratios are depicted in Fig. A1. The surplus of gamma radiation from the noble gas daughters compared to that from the gases is evident. The energy dependency of the daughter ratios is caused by deposition which effects only the C_2 concentrations.

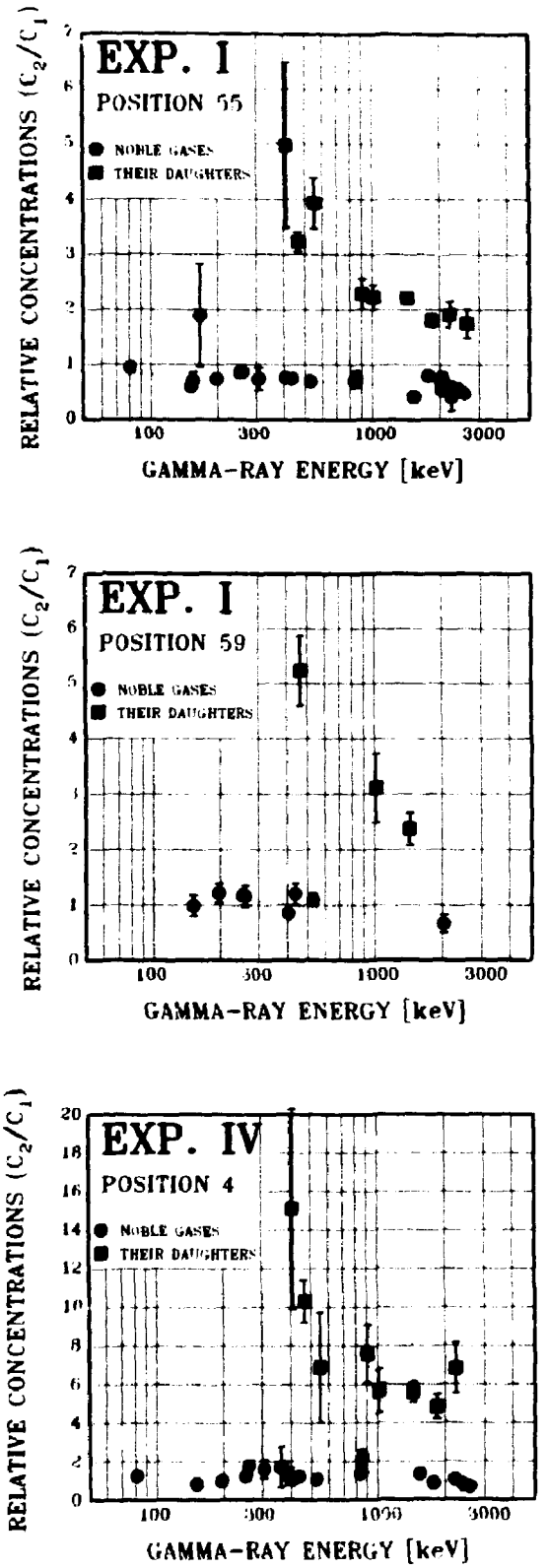

Fig.A1. Ratios of radionuclide concentrations, C_2/C_1, in the air at three measurement positions. The data are from Table A4, A5 and A6.

Table A4. Estimated radionuclide concentrations, C_1 and C_2, in air at experiment I, position 55. C_1 is derived from the SF_6-measurements and C_2 is derived from the gamma-spectrometric measurements and the semi-infinite cloud model.

Isotope	Energy (keV)	C_1 (Bq/m^3)	C_2 (Bq/m^3)	C_2/C_1
Kr 85	151	17.6	10.7±0.5	0.61±0.03
-	305	-	13.0±3.4	0.74±0.20
Kr 87	403	34.0	26.1±1.4	0.77±0.04
-	845	-	25.0±4.9	0.73±0.15
-	2012	-	23.7±4.6	0.70±0.14
-	2555 + 2558	-	16.4±1.8	0.48±0.05
Kr 88	166	40.1	76.0± 37	1.89±0.93
-	196	-	29.5±1.7	0.74±0.04
-	835	-	29.0±4.4	0.72±0.11
-	1530	-	16.9±2.2	0.42±0.06
-	2030	-	21.8±3.1	0.54±0.08
-	2035	-	30.7±4.1	0.77±0.10
-	2196	-	24.6±2.0	0.61±0.05
-	2392	-	22.3±1.1	0.56±0.03
Rb 88	898	11.0	25.1±3.0	2.28±0.27
-	1836	-	19.8±1.3	1.80±0.12
Xe 133	81	25.3	23.7±2.6	0.94±0.10
Xe 135	250	58.5	49.9±0.7	0.85±0.01
Xe 135 m	527	25.7	18.1±0.7	0.70±0.03
Xe 138	154	36.5	25.5±5.5	0.70±0.15
-	258	-	31.9±1.6	0.87±0.04
-	435	-	27.4±1.8	0.75±0.05
-	1768	-	28.8±2.6	0.79±0.07
-	2005	-	25.2±4.3	0.69±0.12
-	2016	-	24.7±3.2	0.68±0.09
-	2252	-	15.4±9.5	0.42±0.26
Cs 138	409	7.1	35.4±1.1	4.98±1.49
-	463	-	22.9±1.3	3.23±0.18
-	547	-	27.9±3.3	3.94±0.46
-	1010	-	15.7±1.5	2.22±0.22
-	1436	-	15.6±0.8	2.20±0.11
-	2218	-	13.5±1.7	1.91±0.23
-	2640	-	12.4±1.9	1.74±0.26

uncertainties from counting statistics only

Table A5. Estimated radionuclide concentrations, C_1 and C_2, in the air at experiment I, position 59. C_1 is derived from the SF_6-measurements and C_2 is derived from the gamma-spectrometric measurements and the semi-infinite cloud model.

Isotope	Energy (keV)	C_1 (Bq/m^3)	C_2 (Bq/m^3)	C_2/C_1
Kr 85 m	151	12.7	12.6±2.4	0.99±0.19
Kr 87	403	24.5	21.0±1.9	0.86±0.08
Kr 88	196	28.8	35.0±5.0	1.22±0.17
Xe 135	250	42.1	49.6±2.7	1.18±0.06
Xe 135 m	527	18.5	20.4±2.0	1.10±0.11
Xe 138	258	26.3	30.4±4.9	1.16±0.19
-	435	-	31.8±5.1	1.21±0.19
-	2016	-	17.4±4.2	0.66±0.16
Cs 138	463	5.1	26.7±3.2	5.23±0.63
-	1010	-	15.9±3.2	3.11±0.62
-	1436	-	12.1±1.5	2.37±0.29

uncertainties from counting statistics only

Table A6. Estimated radionuclide concentrations, C_1 and C_2, in the air at experiment IV, position 4. C_1 is derived from the SF_6-measurements and C_2 is derived from the gamma-spectrometric measurements and the semi-infinite cloud model.

Isotope	Energy (keV)	C_1 (Bq/m^3)	C_2 (Bq/m^3)	C_2/C_1
Kr 85 m	151	10.1	8.3±1.4	0.82±0.14
-	305	-	16.1±4.6	1.59±0.45
Kr 87	403	17.9	18.9±1.5	1.05±0.08
-	845	-	38.9±7.3	2.17±0.41
-	2555	-	12.4±2.0	0.69±0.11
Rb 88	196	22.3	21.8±3.3	0.98±0.15
-	362	-	38.4± 23	1.72±1.03
-	835	-	30.3±4.5	1.36±0.20
-	1530	-	29.9±4.5	1.34±0.20
-	2196	-	23.2±3.3	1.04±0.15
-	2392	-	17.6±1.4	0.79±0.06
Kr 88	898	3.1	23.4±4.7	7.55±1.50
-	1836	-	14.9±1.9	4.82±0.63
Xe 133	81	16.6	20.5±4.6	1.24±0.27
Xe 135	250	32.2	39.9±1.2	1.24±0.04
Xe 135 m	527	16.6	17.9±0.9	1.08±0.05
Xe 138	258	21.2	36.8±2.2	1.74±0.10
-	396	-	26.1±9.1	1.23±0.43
-	435	-	25.6±3.3	1.21±0.15
-	1768	-	18.2±3.5	0.86±0.16
Cs 138	409	1.84	27.8±9.6	15.1 ±5.2
-	463	-	18.9±2.0	10.3 ±1.1
-	548	-	12.6±5.2	6.85±2.85
-	1010	-	10.3±2.1	5.62±1.12
-	1436	-	10.2±0.9	5.56±0.50
-	2218	-	12.5±2.4	6.80±1.31

uncertainties from counting statistics only

Table A7. Estimates of ^{88}Rb- and ^{138}Cs-concentrations, S_A, on the ground at experiment I position 55.

Isotope	Energy (keV)	C_2/C_1 (meas.)	C_2/C_1 (gases)	C_2/C_1 (dep.)	ϕdep. ($\gamma/m^2/s$)	E_1(μh)	y (γ/dis.)	S_A (Bq/m^2)
Rb 88	898	2.28±0.27	0.65±0.02	1.63±0.27	150±35	4.20	0.14	510±119
-	1836	1.80±0.12	0.60±0.03	1.20±0.12	244±33	4.55	0.214	501± 68
Mean								503± 59
Cs 138	409	4.98±1.49	0.71±0.03	4.27±1.49	60±33	3.85	0.0466	669±368
-	463	3.23±0.18	0.70±0.03	2.53±0.18	246±26	3.90	0.307	411± 43
-	547	3.94±0.46	0.69±0.02	3.25±0.46	119±26	3.96	0.1076	559±122
-	1010	2.22±0.22	0.64±0.02	1.58±0.22	211±42	4.25	0.298	333± 66
-	1436	2.20±0.11	0.61±0.03	1.59±0.11	652±65	4.42	0.763	507± 39
-	2218	1.91±0.23	0.58±0.03	1.33±0.23	137±33	4.63	0.152	389± 94
-	2640	1.74±0.26	0.57±0.04	1.17±0.26	67±20	4.72	0.0763	372±111
Mean								395± 24

uncertainties from counting statistics only

The unscattered gamma fluence density from the deposited material is estimated assuming that the airborne daughters are distributed similar to the gases. From a regression line of the data from the gases, interpolation yields C_2/C_1-ratios for the daughter energies, and the difference between these ratios and the measured ratios give the C_2/C_1-ratios from deposition. The total observed unscattered gamma fluence density is split in the same proportion to yield the component from deposited material Φ_{dep}. To arrive at an estimate of the uniform ground concentration S_A, the geometry is assumed to be that of an infinite smooth plane, which permits S_A to be calculated according to

$$S_A = 2\Phi/(E_1(\mu h)\ y),$$

where $E_1(\mu h)$ is the exponential integral of the first-order and the argument is the product of the linear attenuation coefficient of air μ and the height above ground (h = 1 m), y is the gamma yield. For each gamma-ray energy a value S_A is estimated to give a mean concentration for each isotope. The results are shown in Tables A7-A9 and it is noted that the uncertainties from counting statistics alone account for the observed variability between the individually estimated S_A's for each isotope.

Finally, the deposition velocities v_d are estimated from the assumption that a state of equilibrium exists, whereby the rate of deposition equals the rate of decay.

The deposition velocity is calculated from

$$v_d = \lambda\ S_A/C_1,$$

where λ is the decay constant for the isotope. Table A10 shows the deposition velocities calculated from the estimated mean radionuclide concentrations on the ground.

Tabel A8. Estimates of ^{138}Cs-concentration, S_A, on the ground at experiment I, position 59.

Isotope	Energy (kev)	C_2/C_1 (meas.)	C_2/C_1 (gases)	C_2/C_1 (dep.)	ϕdep. ($\gamma/m^2/s$)	E_1(μh)	Y (γ/dis)	S_A (Bq/m^2)
Cs 138	463	5.23±0.63	0.99±0.05	4.24±0.63	297± 67	3.90	0.307	496±112
-	1010	3.11±0.62	0.84±0.09	2.27±0.63	218± 86	4.25	0.298	344±136
-	1436	2.37±0.29	0.77±0.11	1.60±0.31	472±122	4.42	0.763	280± 72
Mean								343± 55

uncertainties from counting statistics only

Table A9. Estimates of ^{88}Rb- and ^{138}Cs-concentrations, S_A, on the ground at experiment IV, position 4.

Isotope	Energy (keV)	C_2/C_1 (meas.)	C_2/C_1 (gases)	C_2/C_1 (dep.)	ϕdep. ($\gamma/m^2/s$)	E_1(μh)	y (γ/dis)	S_A (Bq/m^2)
Rb 88	898	7.55±1.5	1.00±0.06	6.55±1.5	170±62	4.20	0.14	578±211
-	1836	4.82±0.63	0.91±0.08	3.91±0.64	224±55	4.55	0.214	460±113
Mean								486±100
Cs 138	409	15.1 ±5.2	1.11±0.07	14.0 ±5.2	51±31	3.85	0.0466	569±346
-	463	10.3 ±1.1	1.09±0.06	9.2 ±1.1	231±45	3.90	0.307	386± 75
-	548	6.85±2.85	1.07±0.06	5.78±2.85	55±42	3.96	0.1076	258±197
-	1010	5.62±1.12	0.99±0.06	4.63±1.12	161±60	4.25	0.298	254± 95
-	1436	5.56±0.50	0.94±0.07	4.62±0.50	491±82	4.42	0.763	291± 49
-	2218	6.80±1.31	0.89±0.09	5.91±1.31	158±56	4.63	0.152	449±159
Mean								317± 36

uncertainties from counting statistics only

Table A10. Estimates of deposition velocities (m/s).

Isotope	Experiment I position 55	Experiment I position 59	Experiment IV position 4
Rb 88	0.030±0.003		0.10±0.02
Cs 138	0.020±0.001	0.024±0.004	0.06±0.01

uncertainties from counting statistics only

Risø National Laboratory **Risø - R - 495**

A FIELD EXPERIMENT TO VALIDATE ATMOSPHERIC DISPERSION AND DOSE MODELS

S.P. Nielsen*, S.E. Gryning*, O. Karlberg**, E. Lyck*** and S. Thykier-Nielsen*

Date May 1986

Department or group
Health Physics

Groups own registration number(s)

Project/contract no.

Pages 103 Tables 39 Illustrations 18 References 38

ISBN 87-550-1273-6

Abstract (Max. 2000 char.)

Two tracers, sulphurhexafluoride and radioactive noble gases, were released simultaneously from a 110-m stack and detected downwind at distances of 3-4 km. The experiments were made at the Swedish nuclear power plant Ringhals in 1981. The radioactive tracer was routine emissions from unit 1 (BWR). A total of four experiments were made, three in near neutral and one in stable conditions. The one-hour measurements yielded crosswind profiles at ground level of SF_6-concentrations and of gamma radiation from the plume. The measured profiles were compared to profiles calculated with computer models developed at Studsvik Energiteknik and Risø National Laboratory. The comparison showed that the models sometimes underestimate and sometimes overestimate the results, which seems to indicate that the models within their limited accuracy yield unbiased results. The ratios between measured and calculated values range from 0.2 to 3. The measurements revealed a surplus of gamma raditions from the noble gas daughters compared to those from the gases. This was interpreted as due to ground deposition and the estimated deposition velocities ranged from 2 to 10 cm/s.

The meteorological conditions were monitored from a 96-m meteorological tower and from an 11-m mast. Measurements were made of wind speed, wind direction, wind variance and temperatures at different heights, and during each experiment a mini radiosonde was released giving information on a possible inversion layer.

Descriptors - INIS:

COMPARATIVE EVALUATIONS; COMPUTER CALCULATIONS; DEPOSITION; EARTH ATMOSPHERE; ENVIRONMENTAL TRANSPORT; EXPERIMENTAL DATA; FIELD TESTS; GAMMA RADIATION; GAMMA SPECTROSCOPY; METEOROLOGY; NUCLEAR POWER PLANTS; P CODES; PLUMES; RADIOACTIVE EFFLUENTS; RARE GASES; STACKS; SULFUR FLUORIDES; TRACER TECHNIQUES; U CODES

Available on request from Risø Library, Risø National Laboratory, (Risø Bibliotek, Forsøgsanlæg Risø), P.O. Box 49, DK-4000 Roskilde, Denmark.

The SF_6-tracer was injected to the stack prior to the experiments. Air-samples were collected downwind in plastic bags by radio-controlled sampling units. The SF_6-concentrations in the bags were determined with gas chromatography.

Measurements of the gamma radiation from the plume were made with ionization chambers and GM-counters. Furthermore a few mobile gamma spectrometers were available giving information on the unscattered gamma radition, thereby permitting identification of the radioactive isotopes.

Sales distributors:
G.E.C. Gad Strøget
Vimmelskaftet 32
DK-1161 Copenhagen K, Denmark

Available on exchange from:
Risø Library, Risø National Laboratory,
P.O.Box 49, DK-4000 Roskilde, Denmark

ISBN 87-550-1273-6
ISSN 0106-2840